Geophysical Journal International

Geophys. J. Int. (2013) **192,** 38–57 doi: 10.1093/gji/ggs028

An asperity model for fault creep and interseismic deformation in northeastern Japan

Ravi V. S. Kanda,[1,2] Eric A. Hetland[3] and Mark Simons[1]

[1] *Seismological Laboratory, California Institute of Technology* 1200 *E. California Blvd., MC* 252-21, *Pasadena, CA* 91125, *USA. E-mail: rkanda@alumni.caltech.edu*

[2] *Dept. of Geosciences, National Taiwan University No.* 1, *Sec.* 4, *Roosevelt Rd, Taipei,* 10617, *Taiwan*

[3] *Department of Earth and Environmental Sciences, University of Michigan* 1100 *North University Ave, Ann Arbor, MI* 48109, *USA*

Accepted 2012 October 12. Received 2012 October 10; in original form 2012 January 13

SUMMARY

We explore the potential geodetic signature of mechanical stress shadows surrounding inferred major seismic asperities along the Japan-Kurile subduction megathrust. Such stress shadows result from a decrease in creep rates late in the interseismic period. We simplify the rupture history along this megathrust as the repeated rupture of several asperities, each with its own fixed recurrence interval. In our models, megathrust creep throughout the interseismic period evolves according to velocity strengthening friction, as opposed to common kinematic backslip models of locked or partially locked (i.e. coupled) regions of the megathrust. Such backslip models are usually constrained by onshore geodetic data and typically find spatially extensive and smooth estimates of plate coupling, a likely consequence of model regularization necessitated by poor model resolution. Of course, these large coupled regions could also correspond to seismogenic asperities, some of which have not experienced a significant earthquake historically. A subset of existing kinematic models of coupling along the Japan Trench, particularly those that use both horizontal and vertical geodetic data, have inferred a surprisingly deep (∼100 km) locked zone along the megathrust or have called upon complex, poorly constrained megathrust processes, such as subduction erosion, to explain the geodetic observations. Here, we posit two scenarios for distributions of asperities on a realistic 3-D megathrust interface along the Japan-Kurile Trench off NE Japan. These scenarios reflect common assumptions made before and after the 2011 M_w 9 Tohoku-oki earthquake. We find that models that include two shallow *M*9-class asperities (one corresponding to the 2011 Tohoku-Oki earthquake and one offshore of Hokkaido) and associated stress-shadows can explain geodetic observations of interseismic strain along the eastern halves of Honshu and Hokkaido. Specifically, models including localized fault creep can explain most of the observed long-term vertical subsidence in this region during the past century and thus appealing to processes such as deep locking or subduction erosion may not be required.

Key words: Numerical solutions; Seismic cycle; Creep and deformation; Rheology and friction of fault zones; Subduction zone processes; Kinematics of crustal and mantle deformation.

1 INTRODUCTION

Historical records of earthquakes in Japan go back many centuries before instrumental records became available in the 20th century. The size and extents of such historic events can be estimated to first order from intensity estimates based on written records, as well as tsunami deposits. The more recent deployment of a dense geodetic network in Japan (GEONET, since 1994, with roughly 1200 stations having a mean spacing of 20 km; e.g. Sagiya 2004) provides an excellent record of the 3-D deformation field during different stages of the seismic cycle, including coseismic, post-seismic and interseismic periods. Owing to this long recorded history of seismicity, the presence of high-density geodetic and seismic networks for almost two decades, and a well-mapped megathrust interface from offshore seismic surveys, Japan is an ideal place to test models of the seismic cycle.

Over the last century, several large ($M > 7.5$) earthquakes have occurred on the megathrust interface along the Japan Trench, offshore of Tohoku and Hokkaido. Published earthquake source inversions based on seismological and geodetic data suggest that the earthquakes offshore of Miyagi (Miura *et al.* 2006; Umino *et al.* 2006), Sanriku (Tanioka *et al.* 1996; Nakayama & Takeo 1997) and Tokachi (Robinson & Cheung 2003; Hamada & Suzuki 2004; Miyazaki *et al.* 2004; Satake *et al.* 2006) occurred repeatedly over roughly the

same region of the subduction megathrust. However, such events may not be exact repeats of each other (Kanamori *et al.* 2006) and may rupture different but overlapping portions of the megathrust. Nevertheless, seismic rupture zones tend to be relatively compact regions of the megathrust interface (e.g. Yamanaka & Kikuchi 2003, 2004). During the 2011 March 11, M_w 9 Tohoku-oki event, several of these asperities may have slipped together like a single 'giant' asperity, rupturing a significant portion of the megathrust interface (Simons *et al.* 2011). Recent studies show that asperities capable of generating such large tsunamigenic events along the Japan-Kurile Trench may rupture at intervals of the order of 500–1000 yr (e.g. Minoura *et al.* 2001; Nanayama *et al.* 2003; Simons *et al.* 2011), and thus these extremely large earthquakes may not be included in the known earthquake catalogues for northeastern Japan.

In contrast to earthquake source studies which indicate compact asperities (e.g. Yamanaka & Kikuchi 2003; Koketsu *et al.* 2004; Yamanaka & Kikuchi 2004; Miura *et al.* 2006; Sladen *et al.* 2009), estimates of megathrust locking from geodetically measured interseismic deformation produce smooth models that are locked over spatially extensive regions (e.g. Bürgmann *et al.* 2005; Suwa *et al.* 2006; Chlieh *et al.* 2008). Such models assume that net deformation in the over-riding plate is negligible, so that the time-integrated coseismic and transient post-seismic deformation over a sufficiently large number of events exactly cancels the time-integrated deformation over the corresponding interseismic periods. This assumption is mathematically equivalent to imposing slip in the opposite sense to plate convergence (i.e. 'backslip') over the coseismic and post-seismic slip regions (Savage 1983, 1998; Kanda & Simons 2010). The broad and smooth regions of estimated locking in geodetic interseismic models may be a consequence of the lack of model resolution and a resulting need for regularization that is inherent to the use of only onshore geodetic data. Regularization involves a trade-off between the estimated slip distribution and factors such as the choice of data used (e.g., horizontal or vertical velocities), megathrust geometry and its parametrization, assumptions regarding the role of interior faults (Loveless & Meade 2010), and the extent of the fault interface allowed to experience backslip. Alternatively, differences between recognized seismic sources and geodetic estimates of the extent of locking may imply the potential for a large earthquake in the future, as demonstrated, perhaps, by the 2011 M_w 9.0 Tohoku-oki earthquake.

Bürgmann *et al.* (2005) tested the effect of stress-shadows from 'pinned' asperities on horizontal velocity predictions for the subduction zone off Kamchatka for several asperity models. They assumed that all areas outside the asperities slip freely (i.e. with zero resisting shear stress), resulting in a stress-shadow that is primarily located up-dip from each asperity. Since their model does not include fault friction, slip evolution over the seismic cycle—especially down-dip of and laterally (along strike) from these asperities—cannot be modelled. Hetland & Simons (2010) also showed that asperities are surrounded by a 'halo' of very low creep-rates late in the seismic cycle (a 'stress-shadow' effect); however, unlike Bürgmann *et al.* (2005), slip in the regions surrounding these asperities was controlled by an assumed fault rheology in their models. These stress-shadow zones are in essence a physical mechanism for smoothing fault creep, analogous to the broad slip-deficit zones inferred from regularized low-resolution inversions of interseismic geodetic data. An important difference between these two approaches is that the artificial smoothing produced by model regularization in the latter case typically does not include known rupture locations *a priori*.

Here, we investigate whether mechanical processes alone, associated with the decay of coseismic stresses around ruptured asperities in the interseismic period, are sufficient to explain the geodetic data in northern Japan. Specifically, we explore the plausibility of the hypothesis that mechanical coupling of discrete asperities along the Japan Trench megathrust can explain available geodetic observations. We apply the modelling framework of Hetland *et al.* (2010) and Hetland & Simons (2010) to a realistic 3-D megathrust interface of northern Japan [off Tohoku (northern Honshu) and Hokkaido], including a depth dependent rate-strengthening rheology and a relatively well-known sequence of ruptures. To explain the observed GPS velocities over the period 1995–2001, the models require an *M*9-class asperity between the 1978 M_w 7.5 Miyagi-oki and the 1994 M_w 8.1 Sanriku-oki events—a region where significant slip did occur in the 2011 March, M_w 9.0 Tohoku-oki event. These models also require an additional *M*9-class asperity between and updip from, the 2003 M_w 8.1 Tokachi-oki and the 1973 M_w 7.8 Nemuro-oki ruptures. Considering *M*9-class asperities at these suggested locations on the megathrust not only improves the misfits to the horizontal GPS velocities in eastern Honshu and Hokkaido, but also significantly improves agreement with the observed verticals across these regions. Due to the computational costs of our current forward models (Appendix B), the results presented here are based on end-member values of the plausible range of fault frictional strengths. A more refined exploration of the parameter-space will be left for future consideration. In what follows, we briefly discuss our mechanical modelling approach, criteria used to determine asperity extents and rupture intervals, as well as 'spin-up' and 'convergence' of models.

2 FORWARD MODELLING METHODOLOGY

Motivated by estimations of co- and post-seismic slip distributions for *M*8-class earthquakes of the past decade such as the 2003 Tokachi-oki (e.g., Miyazaki *et al.*, 2004), the 2005 Nias (e.g. Hsu *et al.* 2006) and the 2007 Pisco (e.g. Sladen *et al.* 2009; Perfettini *et al.* 2010) events, we assume that the regions of megathrust that experience seismic rupture and aseismic creep are mutually exclusive. (We allow a slight overlap between regions of seismic slip and aseismic creep, as explained below.) We prescribe the localized regions of the fault surface which only slip coseismically at preassigned rupture times ('asperities'), thus making it feasible to incorporate the relatively well known spatio-temporal distribution of large earthquakes, similar to Bürgmann *et al.* (2005). We assume that asperities persist across multiple earthquake cycles and rupture with a characteristic slip. In such a model, aseismic megathrust creep everywhere outside of the asperities at any time is a consequence of long-term plate convergence and determined by cumulative slip from the past rupture history on the fault over a period referred to as the 'spin-up' period. We consider two different asperity distributions off Tohoku and Hokkaido: (i) a distribution capable of producing only *M*7- to *M*8-class events—a scenario which was widely thought to be valid for northern Japan before the 2011 *M*9 Tohoku-oki megathrust event (e.g. Yamanaka & Kikuchi 2003, 2004; Hashimoto *et al.* 2009); and (ii) a two-tier asperity distribution that includes shallow *M*9-class asperities, in addition to those in (i) (e.g. Minoura *et al.* 2001; Nanayama *et al.* 2003; Simons *et al.* 2011). In both scenarios, we do not consider ruptures of moderate to very small magnitudes (e.g. repeating micro-earthquakes) because: (i) It is reasonable to assume that averaged over the seismic cycle timescale, these small asperities rupture more or less passively due to slip from the much larger events; (ii) Unless we are attempting to fit coseismic or

immediate post-seismic geodetic data, onshore surface deformation from such small asperities will be hard to distinguish from the background deformation field (from larger historic ruptures) in active plate boundaries such as the Japan Trench, especially late in the seismic cycle; (iii) Including ruptures from tens to hundreds of such smaller asperities will increase the computational cost without significantly improving our results.

We impose the ruptures in our simulations and thus we do not model the complex dynamics of rupture nucleation, dynamic interaction between asperities, or rupture propagation (see e.g. Rice 1993; Lapusta & Rice 2003; Hori 2006; Kato 2008; Perfettini & Ampuero 2008; Kaneko *et al.* 2010). However, we expect that such effects due to dynamic rupture are short-lived compared to even the smallest asperity rupture interval (30 yr; see Hetland *et al.* (2010)). The spontaneous nature of rupture nucleation in dynamic models of the full earthquake cycle makes it difficult to prescribe known rupture sequences and compare the observed surface deformation field with model predictions. Therefore, we ignore details of the rupture process, and focus on the interseismic period. Other significant assumptions we make include: (i) Ignoring tectonic processes related to the incipient subduction beneath the Okhotsk Plate along the Japan Sea coastlines of Honshu and Hokkaido, (e.g. Apel *et al.* 2006); (ii) Ignoring the role of intraplate faults (e.g. DeMets 1992; Loveless & Meade 2010); (iii) Assuming surface deformation is dominated by localized slip on the fault interface, that is, there is no bulk crustal deformation associated with megathrust earthquakes over a seismic cycle, and especially in the hangingwall (similar to the assumption in kinematic back-slip models; Savage 1983, 1998; Kanda & Simons 2010) and (iv) Ignoring off-fault inelasticity. Given that our model is purely elastic off of the megathrust, any deep off-fault (e.g. viscoelastic) response from past ruptures could map into 'equivalent' fault creep over seismogenic depths.

Below, we address several key issues related to modelling fault-creep resulting from highly non-linear rheologies on a 3-D fault surface. These issues include the construction of the 3-D fault geometry and its discretization, asperity configurations inferred from past rupture history, a plausible distribution of rheological behaviour, and appropriate values for relevant scaling parameters.

2.1 Fault geometry and its numerical discretization

We construct a 3-D geometry of the upper surface of the subducting slab for northeastern Japan using the commercial package gOcad (2010). The constraints on this include bathymetry, seismic reflection surveys and the Wadati-Benioff zone (e.g. Iwasaki *et al.* 2001; Miura *et al.* 2003; Ito *et al.* 2004; Nakanishi *et al.* 2004; Takahashi *et al.* 2004; Miura *et al.* 2005). We isolate the 3-D megathrust interface along the dipping portion of this surface, and discretize the interface with an unstructured triangular mesh (Fig. 1) using the CUBIT finite element geometry-generation/meshing package (Owen 2006). To resolve the rupture stress distributions while maintaining a reasonable size of the numerical discretization, we refine the mesh around each asperity, as well as at major transitions in frictional properties. Dimensions of the resulting triangular patches vary from approximately 1 km in the vicinity of asperities, to roughly two orders of magnitude larger (100–150 km) near the edges of the model domain (Fig. 1). All model parameters (i.e. rheological parameters, stresses, slip, slip-rate, any state-variables, etc.) are either defined or computed at the centroid of the triangular patches comprising the discretized megathrust interface.

When using elastic half-space dislocation solutions to model slip along dip-slip faults (especially during the interseismic period) a typical assumption made is that both the hangingwall and footwall extend up to a horizontal free surface (e.g. Freund & Barnett 1976; Savage 1983; Rani & Singh 1992; Savage 1995, 1998; Cohen 1996). However, the top surface of the downgoing plate in a subduction zone is located at a depth of several kilometres beneath the sea surface. To reconcile this difference between the free-surface locations of the hangingwall and footwall with the boundary conditions of dislocation solutions, the dipping portion of the subducting slab is extended updip from the trench until it intersects mean sea level. This free-surface extension (FSE) consists of all fault patches to the southeast of the trench trace (Figs 1b and c; blue patches in Fig. 2). However, because the FSE is fictitious, we make this surface incapable of supporting significant tractions by making it frictionally much weaker than the megathrust interface downdip.

2.2 Asperity distribution and rupture history

We consider two asperity configuration scenarios along the Japan Trench megathrust: (a) 'APRE' (Fig. 1b): an asperity configuration, made up of *M*7- and *M*8-class asperities widely thought to be representative of the Japan Trench megathrust by studies published prior to the 2011 March M_w9.0 Tohoku-oki event (e.g. Yamanaka & Kikuchi 2003, 2004; Hashimoto *et al.* 2009); and (b) 'APOST' (Fig. 1c): the *APRE* asperity configuration, with additional shallow *M*9-class mega-asperities off Tohoku and Hokkaido—consistent with inferred evidence (e.g. Minoura *et al.* 2001; Nanayama *et al.* 2003; Simons *et al.* 2011) evidence.

We note that there are significant uncertainties in the location and extent of published models of historic rupture asperities (e.g. Yamanaka & Kikuchi 2003, 2004; Hashimoto *et al.* 2009; Uchida *et al.* 2009). Therefore, we take the approximate average of the published asperity centroids to locate our model asperities along the megathrust. We assume that each of the asperities rupture repeatedly with a fixed recurrence interval. Further, we try to honour the time since the latest significant ($M_w > 7.5$) rupture inferred to have occurred on an asperity, as well as the associated moment release, for determining the characteristic slip, rupture interval and size of that asperity. For asperities that are known to have experienced several significant ruptures over the past hundred years (i.e. over the duration of instrumentally recorded history), we use the most recent recurrence time as a fixed recurrence interval (e.g. Miyagi-oki asperity, Appendix A). Asperity size is determined from seismic moment and slip over a fixed rupture interval (eq. A1). For large asperities ($M_w > 8$) whose coseismic slip distributions (and hence spatial extents) are better known, we use eq. (A1) to determine a rupture interval that is consistent with the duration since their last significant rupture. In all cases we ensure that the associated stress-drops are not substantially different from those observed. We summarize the asperity parameters thus obtained in Table 2, and detail the methodology for determining the extents of these characteristic asperities as well as their rupture intervals in Appendix A.

We build the synthetic rupture catalogue retrospectively, starting from the last known rupture on each asperity, resulting in a complex sequence of ruptures characterized by significant temporal variability. Depending on the assumed fixed rupture interval for each asperity, some of the model ruptures prior to the most recent one may not coincide temporally with historical events. However, in most cases, synthetic 'historic' ruptures occur within 5 yr of their actual date. The effect of such small shifts in earlier ruptures does not have a significant impact on surface displacement predictions over the time period of geodetic observations, due to the much

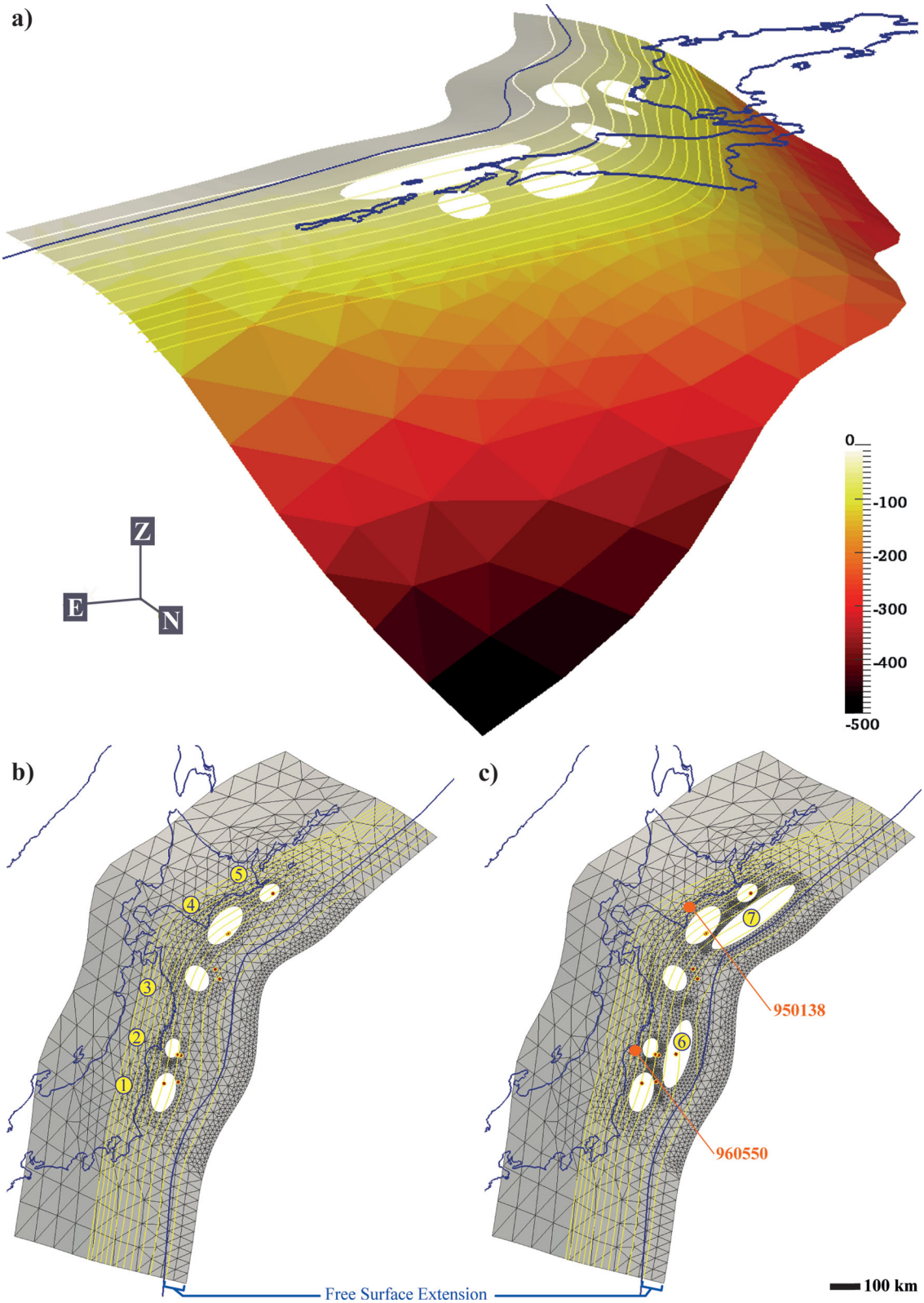

Figure 1. (a) Southeastward perspective view of the 3-D megathrust interface and its discretization (shown for the APOST asperity configuration). (b) APRE asperity configuration: Asperity distribution typically assumed prior to the March, 2011 M_w9 Tohoku-oki earthquake (e.g. Yamanaka & Kikuchi 2003, 2004) and (c) APOST: Plausible asperity configuration based on palaeo-tsunami studies of Minoura *et al.* (2001), and Nanayama *et al.* (2003), as well as the 2011 M_w9 Tohoku-oki event. Yellow numbered circles indicate the asperities used in simulations here: 1, Fukushima; 2, Miyagi; 3, Sanriku; 4, Tokachi; 5, Nemuro; 6, Tohoku-*M*9; 7, Hokkaido-*M*9. Orange circles indicate stations whose synthetic displacement time-series are presented in Fig. 5. Also shown are 10 km depth contours of the inferred megathrust interface (yellow), and the coastlines of northern Japan, southern Kuriles and Shakhailin Island (in b and c), as well as the Japan-Kurile Trench.

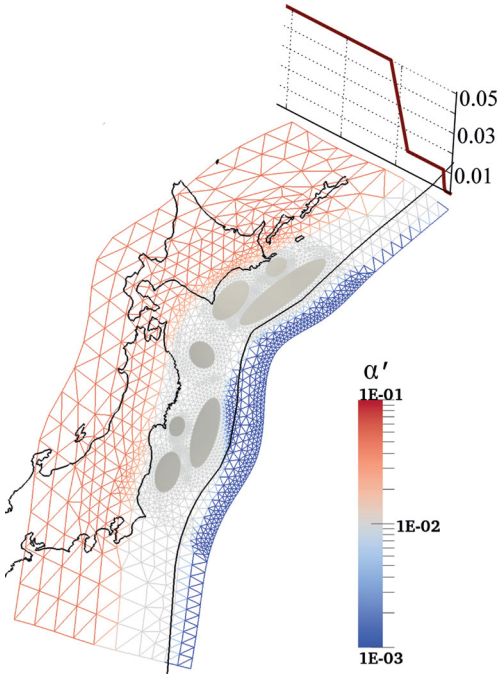

Figure 2. Dimensionless depth-dependent α' distribution used in the strongly rate-strengthening simulations, $\alpha 0.10$. The uniform along-strike α' distribution is shown both as an along-dip (or depth) profile (top panel), as well as a map-view of the megathrust interface, for the APOST asperity configuration. α' is assigned to the centroids of patches shown, which is where tractions are computed. Black lines indicate the coastlines and the trench. Fault patches comprising the free surface extension (FSE, east of the trench) are assigned extremely low frictional resistance (blue).

larger influence of more recent events and the relatively fast decay times of post-seismic processes. Therefore, in choosing our fixed rupture intervals, we place the most emphasis on simulating recent events with reasonable fidelity (see Appendix B for further discussion). As a result of fixing the rupture intervals for each asperity, the most recent rupture sequence included in our simulations (the current rupture sequence or CRS) repeats only once over a much larger time period—600 yr in the APRE scenario, and 9000 yr in the APOST scenario (Fig. S1, and section S.1). In the APRE scenario, the CRS spans the latest ruptures on asperities 1–5 (Table 2 and Fig. 1b), spanning 64 yr between 1936 and 2000 (end of the GPS observation period), while the CRS in the APOST scenario includes all seven asperities (Table 2 and Fig. 1c), whose latest ruptures span 1114 yr between 886 (the synthetic equivalent to the Jogan earthquake of 869; see Appendix A, Section A.6) and 2000. We note that the exact numbers in that appendix are dependent on the assumed/inferred fixed rupture intervals, and are not critical to our primary conclusions.

2.3 Mechanical modelling procedure

Our simulations are based on the mechanical model proposed by Hetland *et al.* (2010) and Hetland & Simons (2010), with modifications associated with using realistic geometry and handling a complex rupture sequence resulting from the *APRE* and *APOST* scenarios described above. Here we summarize the main components of the model, with a focus on the application to realistic faults with non-uniform (i.e. depth-dependent) rate-strengthening rheology. Details such as governing equations, implementation details and model convergence are discussed in Appendix B; Table 1 presents the mathematical notation used throughout this manuscript.

For kinematic consistency, we use a modification to the model of Hetland *et al.* (2010) that simultaneously solves for two components of fault slip (i.e. with variable slip rake over the megathrust). We assume plate convergence having a uniform azimuth across this section of the Japan Trench, which results in the loading rate having varying rake on the non-planar megathrust. This variable rake loading, based on the local strike and dip of the triangular fault patches, results in significant trench parallel strain in the over-riding plate along Hokkaido and the Kuriles, due to horizontal flexure in the megathrust interface due to the northeastward bend in trench-axis in Fig. 1 (and is discussed further in Section 3).

We define the model 'spin-up' period as the time over which fault tractions equilibrate for the imposed loading rate as well as the rupture sequence. Due to ongoing slip associated with past ruptures, the mean tractions over the fault surface fluctuate significantly during spin-up (Fig. 3). The spin-up process in our models is a proxy for rupture history on real fault surfaces—that is, once spun-up, the tractions everywhere on the fault surface depend on all the past ruptures experienced by that fault. However, the average traction over several interseismic periods on the fault surface due to repeated asperity ruptures and continuous far field loading (due to downdip-and along-strike infinite extensions of the fault; and equivalent to backslip) eventually reaches an equilibrium value determined by the fault rheological constitutive relation. Plate loading and resistive stresses are then balanced over most of the fault surface, except in the vicinity of the regularly rupturing asperities. For a given rheology, this equilibrium mean traction corresponds to that which is required to maintain the long-term relative motion between the hanging- and footwall at the steady plate-loading rate, V_0.

The rate-strengthening rheology used here (eq. B5) is characterized by two composite dimensionless rheological parameters: $\rho = f_0/(a-b)$, and $\alpha' = (a-b)\sigma_0 D_0/\mu S_0$, where, f_0 is the static coefficient of friction, a and b are the coefficients of the direct and indirect (state-dependent) dynamic frictional effects, σ_0 the effective normal traction on the fault surface, μ the crustal shear modulus, S_0 the characteristic slip on the asperity and D_0 the characteristic asperity dimension (assumed to be that of the largest asperity in the simulation). Late in the cycle, when most of the fault is slipping at rates close to V_0, the mean dimensionless shear tractions along the fault surface, τ_{eq}, will then equal ρ times the dimensionless strength parameter, α' (i.e. $\tau_{eq} = \rho\alpha' = f_0\sigma_0/\tau_0$; from eq. B5). Thus, τ_{eq} is the ratio of the mean static frictional strength of the fault surface to the characteristic stress induced by a rupture of size, D_0, and average slip, S_0. The mean tractions (and hence, mean slip-rates) at the beginning and end of each spun-up seismic cycle are virtually identical. Also, all patches on the fault would slip by the same amount ($V_0 T_{cycle}$) over the duration of each spun-up seismic cycle, even though some patches (e.g. regions surrounding asperities) may experience most of this slip early in the cycle. Once the model has spun-up, we compute synthetic geodetic velocities from the slopes of the synthetic surface displacement time-series between 1996 and 2001, corresponding to the time span of the GPS data used here (Fig. 5; discussed further in Section 3).

For the results presented below, we follow Rice (1993) and assume effective normal stress, σ_0, to be a constant in space and time. Hetland & Simons (2010) showed that even for the case of a fault with a large static frictional strength, f_0, spatially and temporally variable normal tractions on planar faults induce significant creep only updip of asperities, far from typical geodetic observations.

Table 1. Notation.

a	Coefficient of velocity-dependent term in rate-state frictional parametrization
b	Coefficient of state-dependent term in rate-state frictional parametrization
D_0	Characteristic asperity dimension
f_0	Static friction coefficient
G_{ij}	Surface displacements at location j due to slip on patch i
K_{ij}	Tractions along patch j due to slip on patch i
S_a, S_0	Characteristic coseismic slip on asperity
$\dot{s}$	Slip-rate over a patch
s	Slip over a patch
t	Time
T_R	Time since last rupture prior to the end time of GPS measurements (the year 2000)
u	Surface displacement
V_0, V_P	Plate convergence velocity
V_j	backslip rate
α	Strength parameter for rate-strengthening rheology, $(a–b)\sigma_0$
α'	Dimensionless strength parameter, α/τ_0
ΔT_R	Fixed rupture interval for a characteristic asperity
$\Delta\sigma$	Mean stress drop
ε	Strain
μ	Shear modulus
ρ	Non-dimensional damping parameter, $f_0/(a–b)$
σ_0	Effective normal traction
τ_0	Characteristic coseismic tractions, $\mu S_0/D_0$
τ	Tractions over a patch

Table 2. Summary of asperity parameters for the northern Japan megathrust interface. The columns present asperity name, maximum asperity dimension, D, asperity's elliptical aspect ratio, f, imposed characteristic coseismic slip, s_0, and rupture interval, and the resulting approximate coseismic stress-drop, $\Delta\sigma$. The last column presents the time from the present (here, the year 2000, which marks the end of the time-period over which the observed GPS velocities were computed in Hashimoto *et al.* (2009)) to the most recent earthquake for each asperity in our synthetic catalogue. Appendix A presents details of how these values were derived, and Fig. 1 presents the asperity locations.

#	Region	D (km)	$f(=r_{min}/r_{max})$ (non-dim)	s_0[a] (m)	ΔT_R[b] (yr)	$\Delta\sigma$ [c,d] (MPa)	T_R [yr(date)]
1	Fukushima-oki	140	0.6	7.1	75	10	64 (1938[e])
2	Miyagi-oki	70	0.8	3.8	40	9	22 (1978)
3	Sanriku-oki	100	0.8	2.9	30	5	6 (1994)
4	Tokachi-oki	160	0.6	4.8	50	5	48 (1952)
5	Nemuro-oki	80	0.8	3.8	40[e]	7	27 (1973[e])
6	Tohoku_M9	240	0.35	107	1125	60	1114 (896[f])
7	Hokkaido_M9	350	0.25	48	500[e]	26	348 (1663[e])

[a] $V_P = 9.5 \times 10^{-2}$ m yr^{-1}.
[b] $\Delta T_R \propto (1/A) \propto (1/r^2)$.
[c] $\Delta\sigma \propto s_0 = V_P \times \Delta T_R$.
[d] $\Delta\sigma \propto (1/AD) \propto (1/r^3)$, and, $\Delta\sigma \propto (\Delta T_R)^{1.5}$.
[e] Recurrence interval was assumed (i.e. not based on historical ruptures; see Appendix A).
[f] Not the same exact year as historic rupture (see Appendix A).

They also found that slip rates late in the seismic cycle (i.e. during the interseismic period) were nearly indistinguishable between simulations that included or omitted variations in σ_0 on a planar fault surface. Cumulative slip (and hence, the extent of stress-shadows) in both sets of simulations were nearly identical, because the increased rates in the variable-σ_0 simulations during the post-seismic period were offset by lower rates during the interseismic period.

Real (non-planar) subduction interfaces, such as the one used here, typically have shallow dips updip of asperities. Edge dislocation solutions for slip along such shallow updip patches close to the trench predict sharp localized strains near their updip (ε_{xx}) and downdip (ε_{xy}) limits (e.g. Savage 1983; Aoki & Scholz 2003). As a result, the strain-field associated with them is negligible at distances typical of onshore geodetic stations. Therefore, assuming σ_0 to be constant in space and time may be appropriate for this uppermost section of the subducting interface. However, the deeper portions of the non-planar megathrust have significant interface curvature and may experience localized clamping, especially if rupture induced variable normal tractions, τ_N, are comparable to σ_0. To eliminate an additional parameter from the fault constitutive relations (since these constitutive parameters are themselves not very well constrained), we ignore the spatio-temporal variability of normal tractions here, and use values of σ_0 on the order of 10 times the characteristic shear tractions on the megathrust, τ_0.

Temperature dependence of frictional properties is currently available from experimental studies of gabbro (He *et al.* 2007) and granite (Blanpied *et al.* 1991, 1995), which display remarkably similar behaviour. Due to this similarity, and lack of data on the thermal dependence of frictional properties for the heterogeneous rock types typically expected across the subduction interface, we use a depth dependent α' similar to that for gabbros (Fig. 2). We interpolate this thermal dependence over the modelled thermal structure

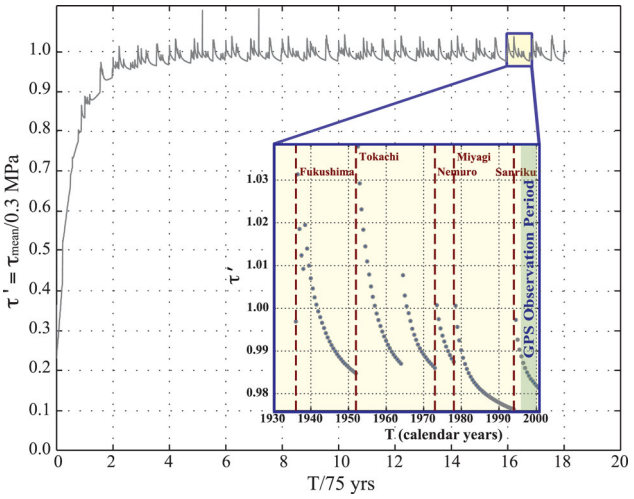

Figure 3. Spin-up of mean dimensionless fault-tractions to a value close to 1.0, and mean tractions over the current rupture sequence (CRS) post spin-up (inset), in the *APRE*-α0.01 model. For the APRE configuration, the CRS repeats every $8\Delta T_{\mathrm{R,\ Fukushima}}$, or 600 yr. The inset corresponds to the mean tractions within the yellow box along the spin-up tractions curve, and shows the modelled historic rupture times for the most recent ruptures on each asperity (dashed red lines). GPS velocities are computed for the time-period corresponding to the years 1996–2000 (green shading in inset).

underneath northern Japan (e.g. Peacock & Wang 1999). As a result of low geothermal gradients in subduction zones as well as a dipping fault interface, the depths to frictional strength transitions are 2–3 times larger than those assumed for continental faults (e.g. in Blanpied *et al.* 1991; Rice 1993). As noted in the previous section, we impose that the artificial FSE is effectively stress-free, by assigning a frictional strength that is two orders of magnitude smaller than the minimum value in the vicinity of the asperities. The final profile assumes a uniform, positive minimum value of the strength parameter, α', over the depth-range corresponding to, but outside of, the inferred seismic asperities. We assume that the depth-profile for the stronger rate-strengthening rheology is identical in shape to that for the weakly rate-strengthening case (Fig. 2), but scaled up linearly in magnitude.

We note that there are large experimental, theoretical and observational uncertainties associated with the depth dependence of frictional strength, and especially, the gradient, $d\alpha'/dz$. These uncertainties primarily result from extrapolating laboratory derived thermal dependence of frictional properties for 'representative' rocks (e.g. Blanpied *et al.* 1991; He *et al.* 2007) to the subduction interface assuming a simple, depth-dependent thermal structure for the downgoing oceanic plate (e.g. Peacock & Wang 1999). However, the depth dependent rheological profiles we use are plausible 'best-guesses' of the real Earth. For example, the depth to the lower transition zone—where the frictional strength increases considerably and ductile behaviour dominates—cannot physically be much deeper than the depths assumed here ($\sim$75 km), based purely on thermal considerations alone (e.g. Hyndman & Wang 1993).

Typical laboratory values of frictional parameters for velocity strengthening materials are: $(a-b) \approx 10^{-2}$ (Blanpied *et al.* 1991; Marone *et al.* 1991), $f_0 \approx 0.1$–1, and $\sigma_0 \approx$ 10–10^2 MPa (Rice 1993; Lapusta & Rice 2003). Thus, typical values for our composite frictional parameters are, $\rho \approx$10–100, and $\alpha \approx 10^5$–10^6 Pa. Assuming $V_0 \approx 10^{-2}$ m yr^{-1}, $S_0 \approx 1$ m, $D_0 \approx 10^4$ m and $\mu \approx 10^{10}$ Pa results in a plausible range for $\alpha' \approx 10^{-2}$–10^{-1}. The number of time steps required for spin-up depends on the mean value of α', and thus on its spatial distribution over the fault surface. Creep over weakly rate-strengthening faults are controlled by coseismic tractions $[\tau_0 > (a-b)\sigma_0]$, and the model spins up quickly. On the other hand, creep over a strongly rate-strengthening fault is controlled by the effective normal stresses $[\tau_0 < (a-b)\sigma_0]$, and requires long spin-up times. For typical values of the damping parameter, ρ, the first term on the right hand side of eq. (5), has only a minor influence on the evolution of post-seismic slip compared to the second term containing α'; however, the value of ρ directly affects the absolute value of tractions attained after spin-up (Hetland *et al.* 2010). Once the model has spun-up, local variations in tractions (and hence slip-rates and cumulative slip) around asperities differ negligibly for different values of ρ. Therefore, we fix the value of ρ equal to a typical value of 10 in all our simulations here.

Here, we only consider simulations with end-member values of α' (0.01, and 0.1), due to computational costs (*cf.* Appendix B). Basic model sensitivity tests were performed for our 3-D megathrust interface using discretizations at different resolutions as well as minor variations in asperity locations. These tests confirmed that there is only a marginal improvement in the solutions for finer mesh resolutions in the vicinity of the asperities, as well as minor perturbations to their locations (Appendix B). We discuss the results of our modelling in the next section.

3 RESULTS AND DISCUSSION

We compare the model predictions for asperity configurations, *APRE* and *APOST*, to observed GPS velocities estimated for the period 1996–2000 (Suwa *et al.* 2006; Hashimoto *et al.* 2009). We refer to each model by the minimum value of the frictional strength parameter, α', from its depth-profile. For instance, α0.01 refers to a rheological model with a minimum value of $\alpha' = 0.01$ in the region surrounding the asperities (grey patches, Fig. 2). We compare results for the frictionless megathrust interface, α0 (similar in concept to Bürgmann *et al.* 2005), with two end-member rheological models, which we refer to as α0.01, and α0.1. In the latter model, α' everywhere on the fault surface is 10 times larger than that in the former. The frictionless model, α0, assumes that only the asperities are locked during the interseismic period, and that the surrounding fault slips without frictional resistance.

Proposed values for the plate-convergence rate across the Japan Trench off Tohoku range from 9.2 to 9.5 cm yr^{-1} (e.g. Heki 2004; Suwa *et al.* 2006; UNAVCO 2011), to 8.3–8.6 cm yr^{-1} (e.g. Loveless & Meade 2010; UNAVCO 2011), depending on whether the Eurasian or Okhotsk plates are used as the reference frame. There could be a 10 per cent uncertainty in plate velocity, or a 5–10° uncertainty in the orientation of the plate convergence vector when using the Okhotsk Plate as the reference (also see eq. A3). Simulations using the smaller, Pacific-Okhotsk, convergence velocities result in smaller characteristic coseismic slip on each asperity, and thus smaller driving model tractions. As a result, modelled slip-rates are lower immediately after each coseismic rupture. So, in addition to the geometric perturbation tests discussed in Appendix B, we also tested simulations of the *APRE* and *APOST* asperity configurations with a 10 per cent lower plate convergence. We found that late in the seismic cycle, however, the stress shadow regions are qualitatively very similar in extent to those for the larger, Pacific-Eurasia, convergence velocity. Due to this similarity, and the fact that we ignore the Okhotsk-Eurasia plate boundary in our simulations, all synthetic interseismic velocities presented here are computed assuming the Pacific-Eurasia plate convergence rate of 9.5 cm yr^{-1},

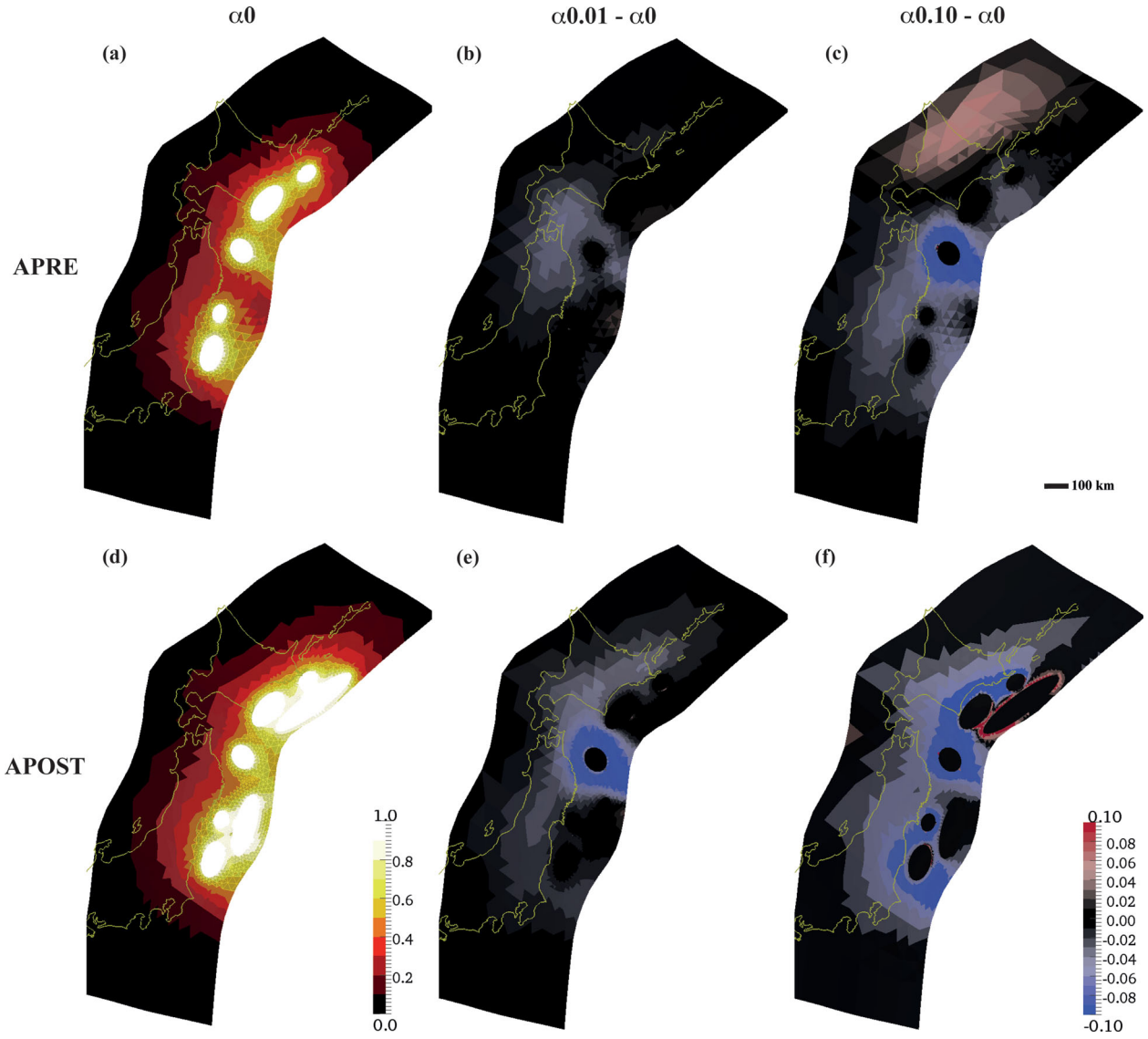

Figure 4. Left column: Absolute slip-deficit (backslip, V_{bs}) rates predicted for the frictionless megathrust interface (a,d). Middle and Right columns: Relative slip-deficit rates of the APRE (b,e) and the APOST (c,f) models for the year 2000, with respect to their frictionless counterparts (a, d, respectively). Slip-deficit rates are normalized relative to the plate convergence rate. Outlines of fault patches experiencing normalized V_{bs} greater than 50 per cent are also shown in (a) and (d). The extent of areas having non-negligible backslip are much larger than individual asperities in all cases. Coastlines are in yellow, and the trench corresponds to the right edge of the megathrust. The free surface extension (FSE) is not shown.

with an azimuth roughly perpendicular to the strike of the trench axis offshore of Tohoku. This trench-normal convergence results in predominantly down-dip slip along the megathrust off the coast of Tohoku. However, due to the sharp change in the strike of the trench southeast of Hokkaido, this plate convergence results in a significant along strike component along the Japan-Kuril trench. Loveless & Meade (2010) propose that this oblique convergence is entirely accommodated (i.e. both co- and post-seismically) by right-lateral slip along the megathrust, even though they include crustal faults which could accommodate such slip.

To use the same reference frame for observations and predictions, as well as facilitate comparison with previously published results (e.g. Suwa *et al.* 2006), we recomputed observed as well as synthetic velocities relative to Geonet Station #940034, located along the central part of the western Tohoku coastline. For the sake of objectivity, and to eliminate any reference-frame uncertainties between the observed and synthetic velocities, we also compare the strain-rate fields and their principal orientations. We use Delaunay triangulation based interpolation of station velocities (adapted for Japan from Hsu *et al.* 2009) to compute the strain-rate fields. The observed GPS velocities and horizontal strain rates relative to the above station (left column of Figs 6 and S2–S7) show significant compression along the western Tohoku coastline. The resulting southeastward horizontal velocities and vertical uplift rates along this coastline are likely due to the incipient subduction of Japan Sea under Honshu. In contrast, vertical velocities over the eastern coastlines of Tohoku as well as northeastern Hokkaido show mostly subsidence.

We compare the slip-deficit (i.e. backslip) rates predicted by the frictionless model to the end-member *APRE* and *APOST* frictional models for the year 2000 (i.e. 'backslip' rates: $V_{bs} = V_P - V_{t=2000}$), at the end of the period corresponding to the GPS observations in Fig. 4. The most striking feature in all these models is that the area of the megathrust estimated to be experiencing non-negligible V_{bs}

(greater than $0.1V_P$) is much larger than the original asperities that ruptured. These broad interseismic backslip zones, exhibiting local maxima in the vicinity of asperities, are dominated by the 'instantaneous', static stress-shadow effect from pinning the megathrust at asperities (Fig. 4, left column). Post-seismic creep due to the relaxation of rupture induced stresses has a secondary, but significant, effect on the interseismic slip-deficit rate distribution depending on the degree of rate-strengthening (Fig. 4, middle and right columns; $V_{\text{bs, frictional-creep}}$ ~10–15 per cent of $V_{\text{bs, pinning}}$). The extent and distribution of these physically based high V_{bs} zones predicted by our simulations are similar to that estimated for northern Japan from numerical inversions of interseismic geodetic data (e.g. Suwa *et al.* 2006; Loveless & Meade 2011). However, unlike those studies, the apparent slip-deficit in our models extends deeper than the observed seismogenic depths because of the 'stress-shadow' effect of pinned asperities and post-seismic creep, not because the megathrust is actually 'locked' to such depths. Zones of high V_{bs} surrounding asperities late in the seismic cycle are passive, and not resisting plate motion. We note that the depth limit of significant V_{bs} appears to be controlled by the (linear) transition in frictional strength assumed downdip of the asperities (Section 2.2, and Fig. 2). Coincidentally, the depth of this frictional transition is close to the maximum curvature portion of our megathrust interface. Therefore, had we included variable normal tractions associated with ruptures in our simulations, the resulting resistance to slip from any clamping associated with interface curvature (Section 2.2) would have increased V_{bs} downdip of this curvature 'axis'.

As a result of the time-dependent slip rates resulting from frictional resistance on the megathrust, the V_{bs} distribution for a frictional fault at any given time is smaller in area, especially in the vicinity of recently ruptured asperities, compared to that for the corresponding frictionless fault. To illustrate this, we take the difference between the V_{bs} fields of the frictional and corresponding frictionless models for each asperity configuration, for the year 2000 (Fig. 4, middle and right columns). An excess backslip rate (reddish hues in Figs 4b, c, e and f) implies more early-cycle frictional fault creep compared to the frictionless, $\alpha 0$, case; a deficit in backslip-rate (bluish hues in Figs 4b, c, e and f) implies excess ongoing frictional creep (or afterslip) compared to the $\alpha 0$ model. Where present, these regions of ongoing frictional afterslip entirely surround asperities, and indicate areas where rupture stresses have not yet been completely dissipated. The V_{bs} distributions for weak rate-strengthening rheologies result in larger stress-shadows (or smaller afterslip) both downdip and updip of the asperities compared to the strongly rate-strengthening rheologies (Fig. 4)—even when frictional properties are assumed to be uniform over the megathrust interface. For example, frictional afterslip around the Sanriku-oki asperity, whose last rupture (1994) occurred just 2 yr before the GPS observation period (1996–2000), is mostly complete in the *APRE*-$\alpha 0.01$ model (Fig. 4b), in contrast to the *APRE*-$\alpha 0.10$ (Fig. 4c). The *APOST* models exhibit significantly larger regions of frictional afterslip, compared to their *APRE* counterparts (Figs 4e and f vs. Figs 4b and c). Most importantly, the best models (*APRE*-$\alpha 0.01$ and *APOST*-$\alpha 0.10$; middle and right columns of Fig. 6) seem to require a backslip distribution closer to that for the frictionless, *APRE*-$\alpha 0$ model. For instance, adding the differenced *APOST*-$\alpha 0.10$ V_{bs} distribution (Fig. 4f) to that for the frictionless, *APOST*-$\alpha 0$, model (Fig. 4d) results in a more compact distribution like that for the frictionless, *APRE*-$\alpha 0$, model (Fig. 4a; summation not shown). Such non-uniqueness in asperity configurations capable of producing similar V_{bs} distributions, combined with the lack of past rupture history, were perhaps the principal confounding factors in identifying the 'asperity' corresponding to the 2011 March Tohoku-oki event prior to its occurrence.

Vertical velocities and horizontal strain-rates in our simulations are much more sensitive to model parameters (e.g. geometry, asperity configuration, fault frictional strength), compared to horizontal velocities (as noted in Kanda & Simons 2010). Figs 5(a and b) present surface displacement time-series for both end-member *APOST* frictional rheologies at two stations located onshore from the Miyagi and Tokachi asperities (Fig. 1), over three overlapping time-periods: (i) starting at the last model rupture of the Tohoku *M*9 asperity and ending in the year 2000 (CRS time period, left columns); (ii) the seven decades prior to 2000 over which instrumentally based earthquake source estimates are available (middle columns) and (iii) 2000–2015, which includes predictions for the present, and up to 4 yr after the 2011 March *M*9 Tohoku-oki rupture (right column). We do not de-trend the time-series to illustrate that the slope of the displacement time-series depends on both the time-span and temporal resolution of GPS observations. Modelled secular horizontal displacements over the CRS time period show a northwestward trend consistent with the principal convergence direction; modelled secular verticals show subsidence due to the combined stress-shadow of all *APOST* asperities (left columns, Figs 5a and b). Surface vertical displacement time-series display significant transient post-seismic responses only for the weakly rate strengthening, $\alpha 0.10$ models (e.g. bottom–middle panel, Fig. 5a), and typically only for stations proximal to the asperity. A response of similar strength is displayed by the horizontals, but is not as obvious in the top rows of Figs 5(a and b) because of its much larger variation compared to the verticals (bottom rows, Fig. 5). The right column of Figs 5(a and b) is discussed further in Section 3.2.1.

Due to the dominance of asperity pinning stress-shadows during the interseismic period (as noted during the earlier discussion on slip deficit rates), the surface deformation field during the interseismic period due to frictional fault creep alone is correspondingly small ($V_{\text{surface, frictional-creep}}$ ~ 10–15 per cent $V_{\text{surface, pinning}}$). Therefore, while we focus only on frictional models in the following sections, we note that a significant portion of their predicted deformation field is due to asperity pinning. Model predictions and residuals for frictionless as well as frictional *APRE* and *APOST* end-member models are presented in the Supplementary Material section.

3.1 APRE: Pre-2011 asperity configuration predictions

Surface interseismic velocity and horizontal strain-rate fields for frictionless as well as frictional end-member *APRE* fault models are presented in Figs S2–S4, and residuals for the best of the three *APRE* models considered, $\alpha 0.01$ (weakly rate-strengthening), are presented in Fig. 6. The *APRE*-$\alpha 0.01$ model provides better fits to the verticals (by up to 3 or 4 mm yr^{-1}) along the coastline of southern Hokkaido and northern Honshu compared to the *APRE*-$\alpha 0.10$ model, which underestimates the uplift rate (by greater than 5 mm yr^{-1} in northern Hokkaido; middle rows, Figs S3 and S4). This underestimation of uplift rates along the coastline by the *APRE*-$\alpha 0.10$ model is a consequence of excess early-cycle slip deep underneath Hokkaido, as well as the large frictional afterslip zone immediately downdip of the simulated 1994 Sanriku rupture (Fig. 4c). In contrast, the observed horizontal velocity field over eastern Tohoku and Hokkaido can be fit equally well by either of these end-member models (top- and middle-right panels of Figs S3 and S4). Perhaps because we include realistic variable-rake backslip, we fit the horizontals much better in southern Hokkaido, compared to recently published horizontal velocity predictions based

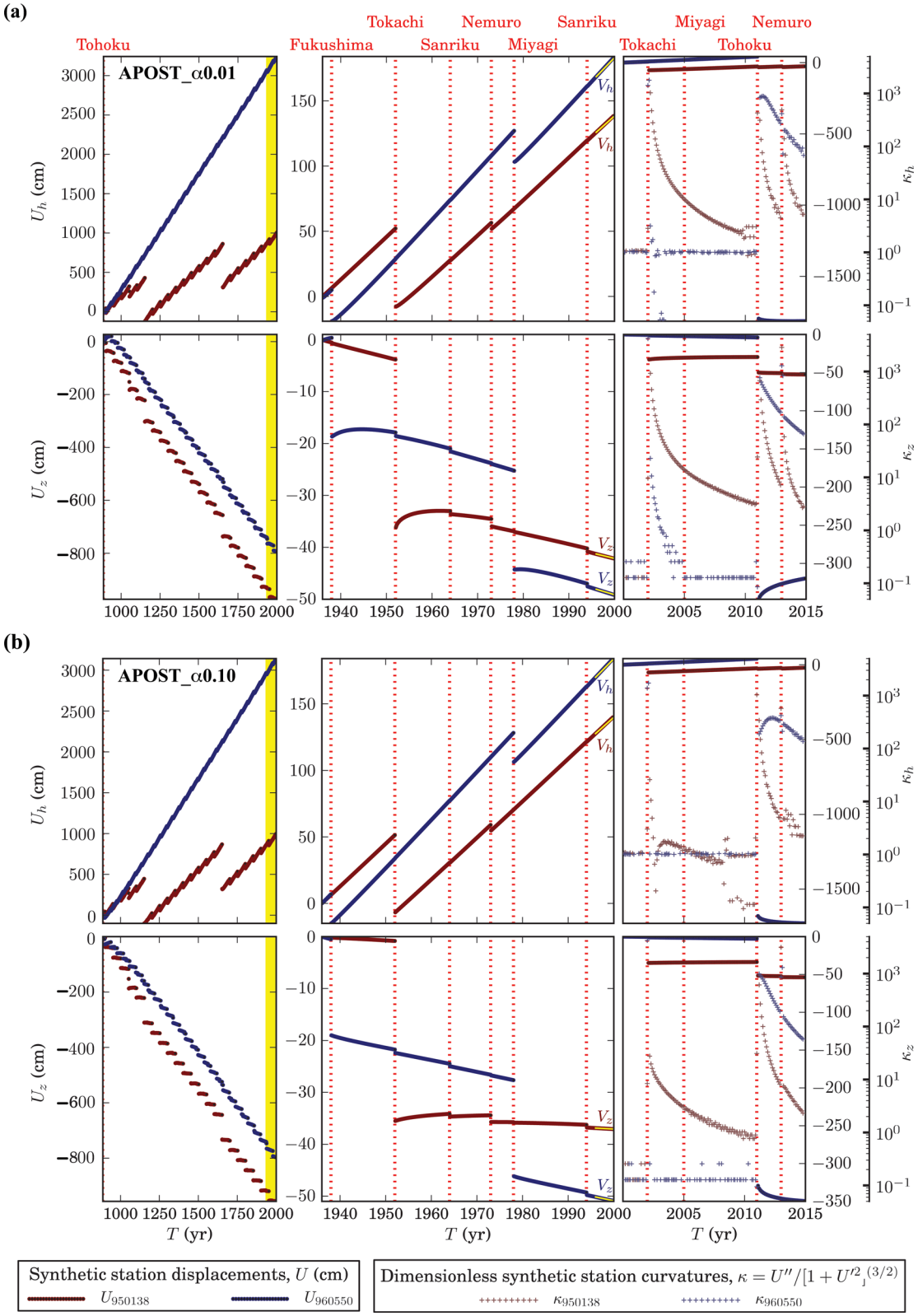

Figure 5. Synthetic surface displacements over the last CRS for coastal stations located landward of the Tokachi asperity (#950138, red lines) and the Miyagi asperity (#960550, blue lines), for the weakly rate-strengthening APOST-α0.01 (a), and strongly rate-strengthening APOST-α0.10 (b) models, over the following time windows: CRS (1125 yr, left column), seven decades prior to the 2011 March Tohoku-oki rupture (middle column, and corresponding to the ruptures presented in Fig. S1b), and 2000–2015 (right column). Both convergence parallel horizontal velocities [top rows of (a) and (b)] as well as vertical velocities [bottom rows of (a) and (b)] are shown. See Fig. 1 for station locations. Yellow shaded patches in the left column indicate the time-span of the respective panels in the middle column. Estimated synthetic GPS velocities over the period of GPS observations, 1996–2000, are presented by thick yellow lines in the middle column.

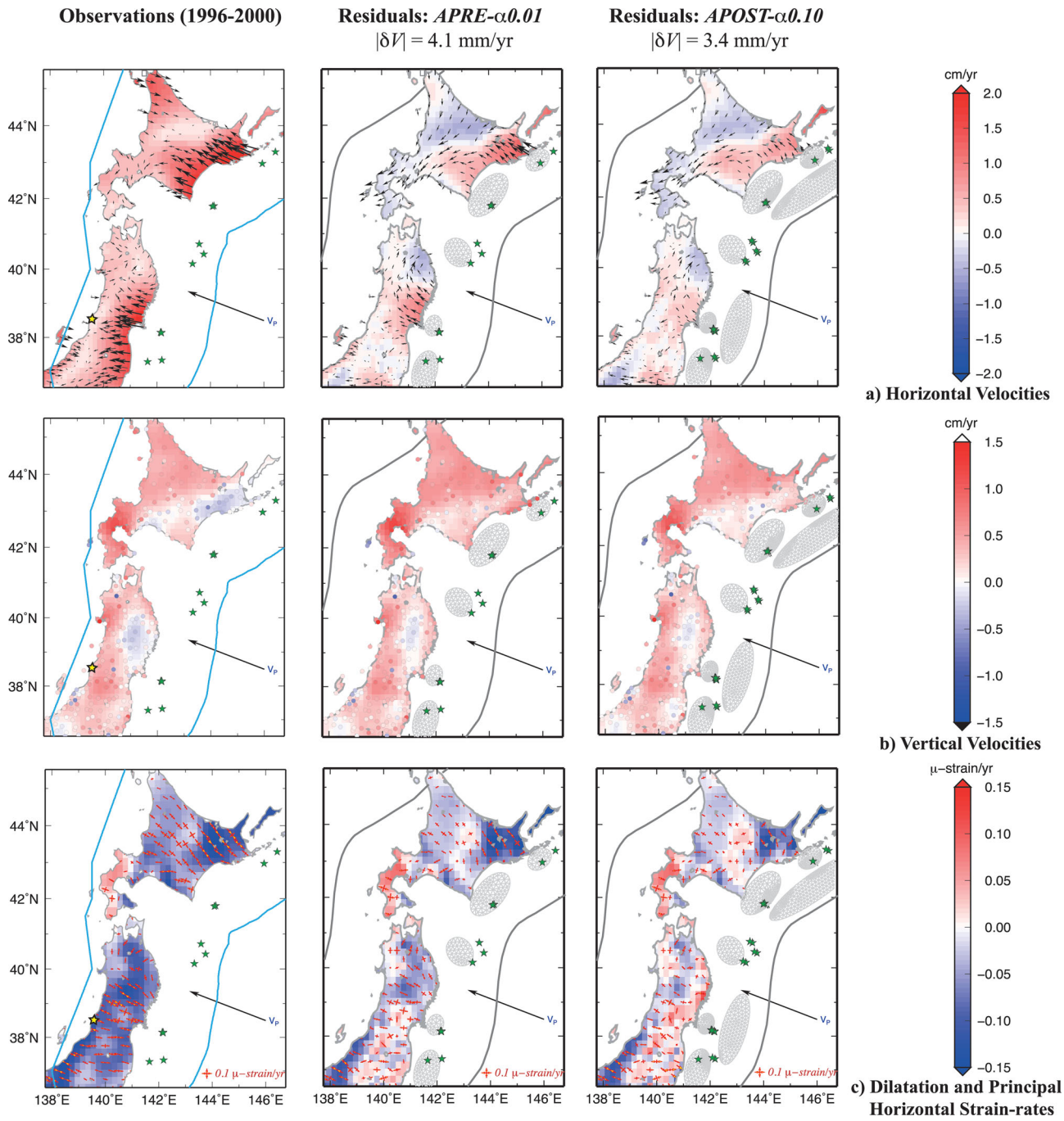

Figure 6. Comparison of GPS observations with model residuals. GPS velocity (a,b) and strain-rate (c) observations (1996–2000, left column). The rest of the columns show residual velocities after removing model contribution from the left column for the best-fit end-member models, *APRE*-α0.01 (middle column), and *APOST*-α0.10 (right column). Plate boundaries are indicated by the blue lines in the left column. Grey lines in the middle and right columns indicate the top and bottom edges of the modelled megathrust interface. Asperities are shown by their component fault patches (grey). Green stars represent the epicentres of major earthquakes during the past 75 yr. Yellow star in the left column represents the reference station (Geonet #940034).

on a sophisticated inversion scheme (e.g. Supplementary Fig. 1, Hashimoto *et al.* 2009). Since horizontals are generally more sensitive to the reference frame chosen for the plate convergence rate, we also compare the strain-rate fields from these horizontal velocities (e.g. dilatation rates presented in part (c) of Figs 6 and S2–S4). Except for a few localized spots (e.g. slightly more compression in regions directly above megathrust areas experiencing downdip afterslip) the misfits in horizontal dilatation rate are quite similar for both rheologies, mirroring our findings for the horizontal velocity field. Therefore, in spite of the lower signal-to-noise ratio of vertical velocities, their sensitivity to fault rheology makes this component much more important compared to horizontals for inferring fault rheological distribution over the seismic cycle timescale (10^3–10^4 yr).

While the global misfit of the *APRE*-α0.01 model is ~20 per cent better than that for the *APRE*-α0.10 model, both models show significant misfits over several geographic areas (middle column of Fig. 6). Much of the geodetic observations along the western

coastline of these islands cannot be explained by slip along the Japan megathrust alone. These residuals along the west coast result from ignoring: (i) incipient subduction in Japan Sea, between the Eurasian (or Amur) and Okhotsk plates and the ensuing distributed compression across western Tohoku & Hokkaido (e.g. Aoki & Scholz 2003; Townsend & Zoback 2006); (ii) strain partitioning along interior crustal faults (e.g. Loveless & Meade 2010); (iii) off-fault processes such as subduction erosion (Heki 2004) which may affect the verticals (a topic we will return to in the next section) and/or (iv) long-lasting regional deformation transients associated with viscoelastic relaxation (e.g. Pollitz *et al.* 2008), which may affect the horizontals.

Northeastern Hokkaido exhibits some of the largest residuals in the APRE models. The large positive misfits in both horizontals and verticals in northeastern Hokkaido, onshore from the Nemuro asperity (middle panel of Figs 6a and b; right panels of (a, b) in Figs S2–S4) suggests that the APRE configuration may be missing a seismically coupled region somewhere in between, and updip from, the two northernmost asperities. A further argument for this missing asperity is the fact that the more complex crustal block models of Loveless & Meade (2010) do not require additional interior strike-slip motion along the western boundary of the Kurile sliver plate (e.g. DeMets 1992). The region where an additional asperity is needed coincides with the location of a potential shallow multisegment mega-asperity in this region inferred by Nanayama *et al.* (2003) from tsunami deposits (Appendix A). Additional misfit in this region may be due to ignoring the effects of the large 1994 *M*8.1 Shikotan intraplate earthquake (e.g. Kikuchi & Kanamori 1995), which occurred just northeast of our model domain.

The APRE models also result in systematic misfits in eastern Tohoku between the Fukushima and Sanriku asperities. These misfits are most apparent in the approximately radial pattern exhibited by the purely compressive principal strain-rate residuals extending northwest and southwest of the Miyagi asperity [Figs 6 and S2–S4 (c)]. As in Hokkaido, these residuals indicate another missing seismically coupled region somewhere in between, and updip from, the two southernmost asperities. In fact a significant region of high-slip observed during the 2011 M_w 9 Tohoku-oki earthquake lies exactly in this region (Simons *et al.* 2011).

Another significant misfit region is Central Honshu (southern Tohoku), with the principal residual strains oriented roughly perpendicular to the nearby Eurasia (Amur)–Okhotsk plate boundary. Several studies have argued that permanent horizontal deformation in central Honshu, beyond that inferred from cyclic subduction zone megathrust ruptures, is related to the motion of the Eurasian (or Amurian) Plate with respect to northeastern Honshu (e.g. Henry *et al.* 2001; Townsend & Zoback 2006; Loveless & Meade 2010). The inferred direction and magnitude of excess horizontal deformation (approximately 1.5–2 cm yr^{-1}) in these studies agrees reasonably well with our estimated horizontal residuals over this region.

3.2 APOST: Post-2011 shallow *M*9-class asperity configuration

We find that including additional shallow *M*9-class asperities off Hokkaido and Tohoku, as suggested by the *APRE* model residuals, results in an improvement in data misfits. The stress-shadows resulting from the pinning of these *M*9 asperities reduce misfits to interseismic observations in the eastern portions of Tohoku and Hokkaido, because of additional subsidence as well as horizontal convergence all along the eastern coastline (compare the middle and right columns of Figs S2 and S5). When rate-strengthening friction is present, the Tohoku *M*9 asperity results in an additional reduction in horizontal residuals along the northern-to-central Tohoku coastline, compared to the corresponding APRE model [right panel of (a) in Figs S6 and S7 vs. Figs S3 and S4, respectively]. A similar effect is observed in northeastern Hokkaido, especially for the strongly rate-strengthening *APOST*-α0.1 model. As a result, the *APOST*-α0.1 model fits observations ~25 per cent better than even the best APRE model (*APRE*-α0.01) or the *APOST*-α0.01 model, in spite of the large misfits along the western halves of Hokkaido and Tohoku (compare $\|\delta V\|$ in the last two columns of Fig. 6; as well as the last columns of Figs S4, S6 and S7). In contrast to the APRE models, the principal residual dilatation-rates in southeastern Hokkaido and eastern Tohoku display neither pure-compression, nor a systematic radial pattern in their orientations (compare last two panels of (c) in Fig. 6). Furthermore, residual dilatation-rates along these coastlines are significantly smaller for the *APOST* models [nearly isotropic; see Figs S5–S7 (c)] compared to those for the *APRE* models. The overall reduction in all of the above residuals suggests that inclusion of the two shallow *M*9-class asperities is sufficient to explain most of the observed surface deformation in this region.

Geodetic surveys of Japan based on 100-yr levelling data (e.g. Yoshii 2005) as well as GPS data over the last decade of the 20th century (e.g. Heki 2004; Suwa *et al.* 2006 and left-centre panels of Figs 6 and S2–S7) indicate that a significant portion of the Pacific coastline of Tohoku and Hokkaido has been experiencing persistent subsidence relative to the Eurasian Plate over the past century. Slip-deficit rate inversions using simple dislocation models require very deep 'locked' zones to match the observed 'hingeline' (e.g. Suwa *et al.* 2006). Due to the implausibility of such a deeply locked fault, it has been argued that this subsidence is perhaps related to ongoing subduction erosion (Aoki & Scholz 2003; Heki 2004; Hashimoto *et al.* 2008). However, our results [right panels of Figs 6 and S5–S7 (b)] imply that the existence of shallow *M*9-class asperities could be a plausible, and much simpler explanation for this persistent subsidence observed along the eastern coasts of Hokkaido and Tohoku over this long time period.

The above results imply that when shallow mega-asperities are included offshore from Hokkaido and northern Honshu, the observations are better described using a model with stronger rate-strengthening friction than that suggested by the *APRE* models. As noted previously, stronger rate strengthening in the *APOST* fault model results in significant afterslip around all asperities later-on in the cycle, compared to only around recent ruptures in the weaker rate-strengthening case [e.g. Sanriku asperity; compare Fig. 4 (f) with (e)]. There is thus a strong trade-off in our models between shallow pinning (i.e. asperity configuration) and deep post-seismic slip (i.e. fault frictional properties). This strong trade-off illustrates the importance of prescribing the correct fault and asperity geometry as well as rupture history when inferring long-term fault rheology.

Significant misfits persist along the western coasts of Tohoku and Hokkaido in *APOST* models, irrespective of fault rheology (last column of Fig. 6), due to the same reasons identified for the *APRE* models in this region (i.e., ignoring incipient subduction off the Japan Sea coastline; see Section 3.1). In addition, significant misfits exist in the northeastern corner of Hokkaido for even the *APOST*-α0.1 model, similar in distribution to the misfits for the best APRE model (though smaller in magnitude). The similarity of the spatial distribution of misfits in the two asperity configurations

in this region points to a common source, such as ignoring the effects of the large 1994 *M*8.1 Shikotan island intraplate earthquake (e.g. Kikuchi & Kanamori 1995), which occurred just northeast of our model domain, or inaccurate geometry and/or location of the Nemuro asperity (e.g. the asperity may be larger and/or deeper). The systematic overestimation of subsidence-rates and underestimation of compressive strain-rates in northeastern Tohoku and southeastern Hokkaido, suggest that even stronger rate-strengthening friction is required along the megathrust in this region, perhaps related to the large curvature of the interface associated with the sharp bend in the trench axis there. Further, the excess horizontal velocities predicted by the *APOST-α*0.1 model in northeastern Tohoku seem to indicate the Sanriku-oki asperity may actually be located slightly shallower along the megathrust interface. Such a shallower Sanriku asperity would also minimize the overestimation of subsidence-rate in this region by localizing high strain-rates closer to the trench. A further concern is the likely along-strike variation of frictional parameters, which we have completely ignored here. Addressing these trade-offs will require a higher resolution parameter space exploration, and ultimately, solving the inverse problem of estimating plausible fault rheological distributions with a given configuration of asperities. In addition, given the first-order effect of pinning the asperities (e.g. Fig. 4; and Bürgmann *et al.* 2005), source parameters such as coseismic slip distribution (Section 3.2.1), asperity aspect ratio and centroid may also need to be included as parameters for inversion.

3.2.1 Predictions of transient afterslip and surface deformation post-Tohoku-oki

As an example of the types of analysis that can be done in the future with our methodology, we estimate both afterslip and post-seismic surface displacements over a 3 yr period following a simulated Tohoku_*M*9 rupture for both end-member APOST models (Fig. 7). Note that these results are for the end-member rheologies discussed above, and are not optimized to fit any post-seismic data. A striking feature of the post-seismic response is the compactness of the deformation fields predicted by the *APOST-α*0.1 model compared to the *APOST-α*0.01 model, especially after the first year following rupture, both along the megathrust (top panels, Figs 7b and c), as well as at the surface (middle & bottom panels, Figs 7b and c). Both models predict significant cumulative afterslip during the first year following a simulated Tohoku *M*9 rupture in the immediate vicinity of this asperity. In subsequent years, however, cumulative afterslip is peaks to the northwest of the asperity (i.e. downdip; 'S' in the top panels, Figs 7b and c) irrespective of the fault rheology. Cumulative afterslip over the first year following rupture is of the order of 10s of metres for both *APOST* end-member models. Over the subsequent couple of years (i.e. years 1–3), however, the peak cumulative afterslip predicted by the *APOST-α*0.1 model (∼ 2 m) is nearly four times that for the *APOST-α*0.01 model (right column, Figs 7b and c); however, the afterslip distribution during this period is significantly more compact for the former case. In

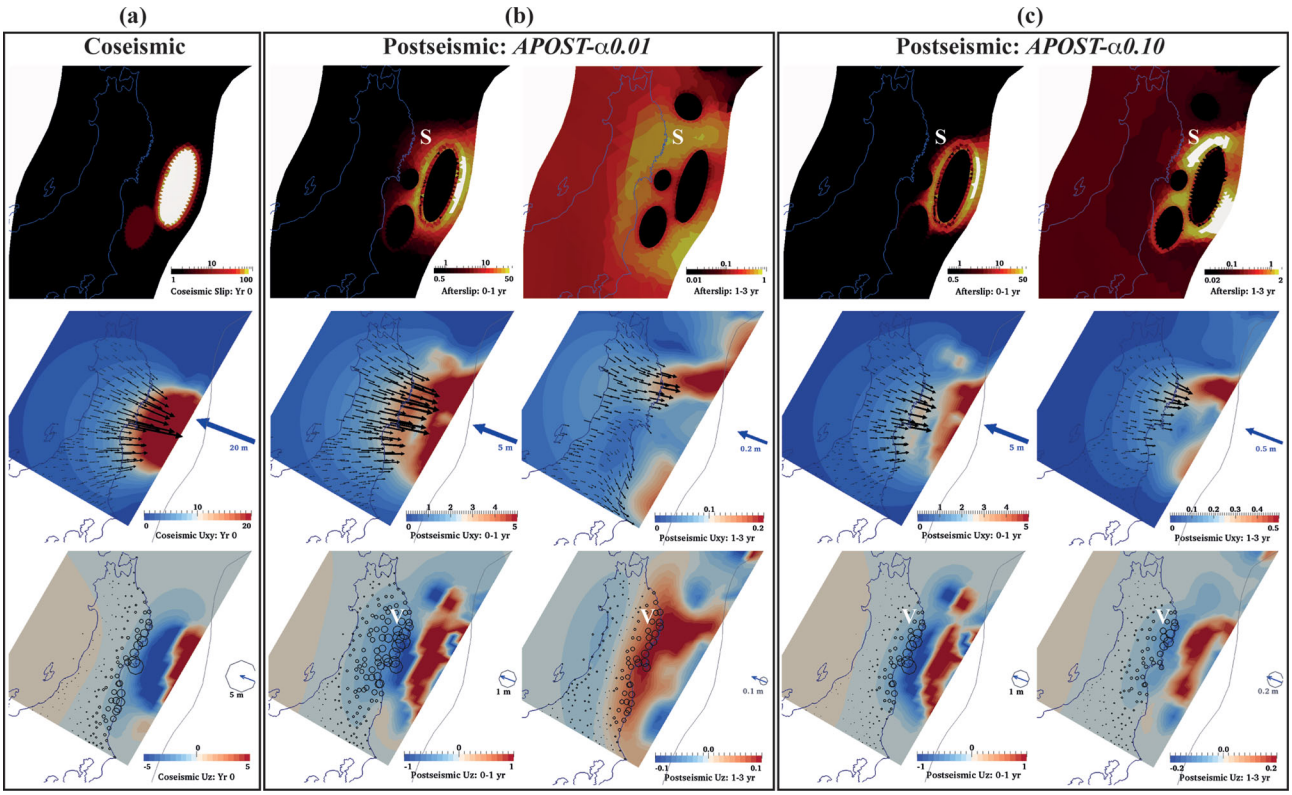

Figure 7. Coseismic (a) and Post-seismic response of the weakly (b, α0.01) and strongly (c, α0.10) rate-strengthening *APOST* frictional models over 3 yr following a simulated Tohoku-*M*9 rupture. Shown are fault creep (top row), and surface horizontal (middle row) and vertical (bottom row) displacements. Due to the significantly different post-seismic response magnitude, the first year after rupture [first column of (b) and (c)] is shown separately from the cumulative slip over the two subsequent years [i.e. years 1–3, second column of (b) and (c)]. Colourbars were chosen for ease of readability of the plots. Blue vectors in the middle row represent the scale for horizontal displacements in the plate convergence direction. Black circles in the bottom row represent the scale for vertical displacements, with a thin blue arrow indicating only the plate convergence direction. Areas denoted by 'S' on the fault surface [top row of (b, c)], and 'V' at the free-surface [bottom row of (b,c)] are discussed in Section 3.2.1.

comparison, recent studies of post-seismic deformation following the 2011 March *M*9 Tohoku-oki rupture based on regularized (e.g. Ozawa *et al.* 2011) as well as a Bayesian (e.g. Ortega Culaciati *et al.* 2011) inversions of geodetic data infer peak afterslip of ~ 0.5 to 1 m during the first 2 weeks after rupture. Further, in both cases the afterslip distribution peaks to the west and northwest (i.e. downdip) of the inferred coseismic slip area, similar to our *APOST*-α0.01 model. The most likely solution estimated by the Bayesian approach is consistent with the sharp circum-asperity peak in cumulative afterslip predicted by our physical models, especially downdip of the coseismic rupture area; however, the regularized inversion does not detect such sharp circum-asperity afterslip. Also, neither study detects significant afterslip updip of the coseismic rupture, probably because the inferred coseismic rupture extends all the way to the trench, in contrast to our models. On the other hand, the nearly identical sharp circum-asperity peak in frictional afterslip present in both end-member models during the first year following rupture could be an artefact of the sharp gradients in our imposed coseismic rupture slip distribution (Appendix B).

Strong transients are observed in the synthetic time-series of most stations along the Tohoku coastline following the simulated *M*9-class rupture (right column, Figs 5a and b). It is also interesting that the two end-member rheologies here predict vertical post-seismic velocities of opposite sense along the east coast of Tohoku in the years immediately following the *M*9-class rupture (blue time-series in the bottom-right panels of Figs 5a and b; 'V' in the top panels of Figs 7b and c). Early post-seismic velocities presented in Ozawa *et al.* (2011) indicate a broad region of uplift along much of the Tohoku coastline, similar to our *APOST*-α0.01 model after the first year following rupture. However, the magnitude and sense of post-seismic surface displacements predicted by our *APOST* models during the first year may not be realistic due to the artificially sharp gradients in our imposed rupture slip distribution. In fact, subtracting out the sharp high-afterslip 'ring' (yellow-white zones of afterslip > 20 m) would result in a more diffuse slip distribution. Such a distribution would shift the hingeline (zone of zero vertical uplift-rate) landward, resulting in post-seismic uplift along the coastline (similar to that predicted for the 1–3 yr period). Nevertheless, post-seismic data seem to favour the weakly rate-strengthening model, in contrast to the interseismic data discussed in the previous section. However, given low sensitivity of our frictional models during the interseismic period, post-seismic data are probably the key to constraining long-term fault rheological properties. Fitting both the interseismic GPS observations as well as post-seismic displacements following the 2011 Tohoku-oki rupture may require rate-strengthening parameters somewhere in between these two end-member cases.

We also computed the dimensionless curvature of the synthetic time-series for the years 2000–2015 ('+' symbols in the last columns of Figs 5a and b). Not surprisingly, peak curvature immediately after rupture is an order of magnitude larger for the *APOST*-α0.01 model compared to the *APOST*-α0.1 model. For either model, the large curvature estimated for the immediate post-seismic period decays rapidly by 2–3 orders of magnitude over the first few years, consistent with the predicted cumulative afterslip distributions (top panels of Figs 7b and c). For short interrupture time intervals, curvature does not become zero (indicative of 'secular' interseismic velocity) during the preseismic period for subsequent ruptures (e.g. preseismic period for the 2011 *M*9 Tohoku-oki rupture; red time-series in the bottom-right panels of Figs 5a and b). The change in curvature over the preseismic period for the simulated 2003 *M*8 Tokachi-oki event is not apparent in these plots because of the much larger post-seismic curvature change following that rupture. Models such as these, along with post-seismic observations over the next several years from the dense GEONET GPS network, would help constrain the long-term, large wavelength rheological structure along the megathrust interface off Japan.

4 CONCLUSIONS

The results presented above demonstrate an alternative to conventional kinematic models that have been used to investigate deformation during the post-seismic to interseismic time-periods. In a manner similar to the apparent locking of large regions of the megathrust required by interseismic geodetic data inversions (e.g. Suwa *et al.* 2006), the forward models presented here require long-wavelength regions of significant slip-deficit along the megathrust interface to explain current geodetic velocities. These slip-deficit regions around asperities correspond to stress-shadows in the vicinity of asperities, due to two phenomena: (i) static, 'instantaneous' stress-shadows resulting from pinning the megathrust at these asperities, and (ii) transient afterslip due to the rapid dissipation of coseismic stresses early in the seismic cycle. We find that such coupling can explain the first-order pattern of both horizontal and vertical geodetic velocities along the eastern half of northern Japan. Hence, the hypothesis that mechanical coupling due to inferred asperities alone is sufficient to explain available geodetic observations above the Japan megathrust appears to be plausible. Further, good fits to observations by the APOST models suggest that shallow *M*9-class asperities could provide an alternative for the observed long-term subsidence of the eastern coastline of northern Japan over the past century. These *M*9-class asperities include the region that ruptured in the 2011 *M*9 Tohoku-oki earthquake (e.g. Simons *et al.* 2011), as well as an asperity updip of the source region of the 2003 *M*8.1 Tokachi-oki earthquake (e.g. Robinson & Cheung 2003; Koketsu *et al.* 2004; Satake *et al.* 2006). We note that such large characteristic asperities may actually be collections of closely spaced smaller asperities (Simons *et al.* 2011), which may rupture in multiple *M*8- or *M*7.5-class events rather than as a single *M*9-class event. We also show that unless there is a large gap ($\sim$ a decade or longer) between significant megathrust ruptures ($M > 7$), surface displacement time-series do not attain true secular interseismic velocities.

We stress that what we presented here is only a forward modelling exercise, and thus, the reasonable fits to observations based purely on end-member rheological models are by no means unique, but nonetheless satisfying. However, given that stress shadows from frictional afterslip are only a secondary contribution to the interseismic deformation field, compared to the impact of pinning asperities (i.e. as shown in Bürgmann *et al.* 2005), post-seismic observations hold the key to estimating fault rheological properties using such physical models. Also, the strong trade-off between fault frictional properties and the chosen asperity configuration in our models illustrates the first-order importance of prescribing fault and asperity geometry as well as rupture history for complete seismic-cycle simulations with as much fidelity as possible. Given the computational time required for simulations having realistic fault surfaces and multiple asperities with complex rupture sequences, we defer a refined parameter-space search, as well as the inverse problem of inferring fault asperity as well as rheological distribution from geodetic data over the complete seismic-cycle, to future studies.

Our model formulation can be readily extended to estimate fault rheologies from the complete interseismic to post-seismic response of the overriding plate to a specified rupture history. In addition, ruptures on other major regional faults could be included (e.g. those related to incipient subduction in Japan Sea, or interior crustal faults).

Our approach can also be applied to other subduction zones where high-density geodetic data may become available in the near future (e.g. the Sunda Trench off Sumatra or the Peru-Chile Trench). The ability to investigate 4-D velocity field predictions simultaneously at hundreds of stations and over the entire seismic cycle, has the potential to provide valuable insights into the behaviour of subduction zones and therefore the associated seismic hazard. However, a significant improvement in the computational efficiency of these models will be required for such comprehensive analyses to be practical.

ACKNOWLEDGMENTS

We thank Hiroo Kanamori for his insights in estimating the set of characteristic asperities used in our simulations. We thank Yaru Hsu for providing the original strain calculation code which we adapted for Japan. RVSK also thanks Prof. John Suppe for providing computational facilities and financial support to complete the project at the National Taiwan University, Taipei, Taiwan. We also thank Roland Bürgmann and an anonymous reviewer, whose constructive criticism significantly improved the clarity of this manuscript. This is Caltech Seismological Laboratory publication 10070, and Caltech Tectonics Observatory publication 192.

REFERENCES

Abe, K., 1977. Tectonic implications of the large Shioya-oki earthquakes of 1938, *Tectonophysics,* **41,** 269–289.

Aoki, Y. & Scholz, C.H., 2003. Vertical deformation of the Japanese islands, 1996–1999, *J. geophys. Res.,* **108**(2257), doi:10.1029/2002JB002129.

Apel, E.V., Burgmann, R., Steblov, G., Vasilenko, N., King, R. & Prytkov, A., 2006. Independent active microplate tectonics of northeast Asia from GPS velocities and block modeling, *Geoph. Res. Lett.,* **33**(L11303), doi:10.1029/2006GL026077.

Blanpied, M., Lockner, D. & Byerlee, D., 1991. Fault stability at hydrothermal conditions, *Geophys. Res. Lett.,* **18,** 609–612.

Blanpied, M., Lockner, D. & Byerlee, D., 1995. Frictional slip of granite at hydrothermal conditions, *J. geophys. Res.,* **100,** 13 045–13 064.

Bürgmann, R., Kogan, M., Levin, V., Hilley, G.E., Steblov, G. & Apel, E., 2005. Interseismic coupling and asperity distribution along the Kamchatka subduction zone, *J. geophys. Res.,* **110**(B07405), doi:10.1029/2005JB003648.

Chlieh, M., Avouac, J.P., Sieh, K., Natawidjaja, D.H. & Galetzka, J., 2008. Heterogeneous coupling of the Sumatran megathrust constrained by geodetic and paleogeodetic measurements, *J. geophys. Res.,* **113**(B05305), doi:05310.01029/02007JB004981.

Cohen, S.C., 1996. Convenient formulas for determining dip-slip fault parameters from geophysical observables, *Bull. seism. Soc. Am.,* **86,** 1642–1644.

Comninou, M. & Dunders, J., 1975. Angular dislocation in a half space, *J. Elasticity,* **5,** 203–216.

DeMets, C., 1992. Oblique convergence and deformation along the Kuril and Japan trenches, *J. geophys. Res.,* **97,** 17615–17625, doi:10.1029/92JB01306

Freund, L.B. & Barnett, D.M., 1976. A two-dimensional analysis of surface deformation due to Dip-slip faulting, *Bull. seism. Soc. Am.,* **66,** 667–675.

gOcad-Consortium, 2010. gOcad introductionGocad Research Group, Available at http://www.gocad.org/w4/index.php/gocad/presentation10.1093/gji/ggs028.html (accessed 2 November 2012).

Hamada, N. & Suzuki, Y., 2004. Re-examination of aftershocks of the 1952 Tokachi-oki earthquake and a comparison with those of the 2003 Tokachi-oki earthquake, *Earth Planets Space,* **56,** 341–345.

Hashimoto, C., Node, A., Sagiya, T. & Matsu'ura, M., 2009. Interplate seismogenic zones along the Kuril-Japan trench inferred from GPS data inversion, *Nat. Geosci.,* **2,** 141–144.

Hashimoto, C., Sato, T. & Matsu'ura, M., 2008. 3-D simulation of steady plate subduction with tectonic erosion: Current crustal uplift and free-air gravity anomaly in northeast Japan, *Pure appl. Geophys.,* **165,** 567–583.

He, C., Wang, Z. & Yao, W., 2007. Frictional sliding of gabbro gouge under hydrothermal conditions, *Tectonophysics,* **445,** 353–362.

Heki, K., 2004. Space Geodetic observation of deep basal subduction erosion in northeastern Japan, *Earth planet. Sci. Lett.,* **219,** 13–20.

Henry, P., Mazzotti, S. & Pichon, X.L., 2001. Transient and permanent deformation of central Japan estimated by GPS. 1. Interseismic loading and subduction kinematics, *Earth planet. Sci. Lett.,* **184,** 443–453.

Hetland, E.A. & Simons, M., 2010. Postseismic and interseismic deformation due to fault creep II: Transient creep and interseismic stress shadows on megathrusts, *Geophys. J. Int.,* **181,** 99–112.

Hetland, E.A., Simons, M. & Dunham, E.M., 2010. Postseismic and interseismic deformation due to fault creep I: model description, *Geophys. J. Int.,* **181,** 81–98.

Hori, T., 2006. Mechanisms of separation of rupture area and variation in time interval and size of great earthquakes along the Nankai Trough, southwest Japan, *J. Earth Simul.,* **5,** 8–19.

Hsu, Y.-J. *et al.*, 2006. Frictional afterslip following the 2005 Nias-Simeulue earthquake, Sumatra, *Science,* **312,** 1921–1926.

Hsu, Y.-J., Yu, S.-B., Simons, M., Kuo, L.-C. & Chen, H.-Y., 2009. Interseismic crustal deformation in the Taiwan plate boundary zone revealed by GPS observations, seismicity, and earthquake focal mechanisms, *Tectonophysics,* **479,** 4–18.

Hyndman, R.D. & Wang, K., 1993. Thermal constraints on the zone of major thrust earthquake failure: the Cascadia subduction zone, *J. geophys. Res.,* **98,** 2039–2060.

Ito, A., Fujie, G., Tsuru, T., Kodaira, S., Nakanishi, A. & Kaneda, Y., 2004. Fault plane geometry in the source region of the 1994 Sanriku-oki earthquake, *Earth planet. Sci. Lett.,* **223,** 163–175.

Iwasaki, T. *et al.*, 2001. Extensional structure in northern Honshu arc as inferred from seismic refraction/wide-angle reflection profiling, *Geophys. Res. Lett.,* **28,** 2329–2332.

Kanamori, H., 1971. Focal mechanism of the Tokachi-Oki earthquake of may 16, 1968: contortion of the lithosphere at a junction of two trenches, *Tectonophysics,* **12,** 1–13.

Kanamori, H. & Anderson, D.L., 1975. Theoretical basis of some empirical relations in seismology, *Bull. seism. Soc. Am.,* **65,** 1073–1095.

Kanamori, H., Miyazawa, M. & Mori, J., 2006. Investigation of the earthquake sequence off Miyagi prefecture using historical seismograms, *Earth Planets Space,* **58,** 1533–1541.

Kanda, R.V.S. & Simons, M., 2010. An elastic plate model for interseismic deformation in subduction zones, *J. geophys. Res.,* **115**(B03405), doi:10.1029/2009JB006611.

Kaneko, Y., Avouac, J.-P. & Lapusta, N., 2010. Towards inferring earthquake patterns from geodetic observations of interseismic coupling, *Nat. Geosci.,* **3,** 363–369.

Kato, N., 2008. Numerical simulation of recurrence of asperity rupture in the Sanriku region, northeastern Japan, *J. geophys. Res.,* **113**(B06302), doi:10.1029/2007JB005515.

Kikuchi, M. & Kanamori, H., 1995. The Shikotan Earthquake of October 4, 1994: lithospheric earthquake, *Geophys. Res. Lett.,* **22,** 1025–1028.

Koketsu, K., Hikima, K., Miyazaki, S. & Ide, S., 2004. Joint inversion of strong motion and geodetic data for the source process of the 2003 Tokachi-oki, Hokkaido, earthquake, *Earth Planets Space,* **56,** 329–334.

Lapusta, N. & Rice, J., 2003. Nucleation and early seismic propagation of small and large events in a crustal earthquake model, *J. geophys. Res.,* **108,** 2205.

Loveless, J.P. & Meade, B.J., 2010. Geodetic imaging of plate motions, slip rates, and partitioning of deformation in Japan, *J. geophys. Res.,* **115**(B02410), doi:10.1029/2008JB006248.

Loveless, J.P. & Meade, B.J., 2011. Spatial correlation of interseismic coupling and coseismic rupture extent of the 2011 $M_W = 9.0$ Tohoku-oki earthquake, in *Abstract G44A-06 presented at 2011 Fall Meeting*, AGU, San Francisco, California, 5–9 Dec.

Marone, C., Scholz, C. & Bilham, R., 1991. On the mechanics of earthquake afterslip, *J. geophys. Res.,* **96,** 8441–8452.

Meade, B.J., 2007. Algorithms for the calculation of exact displacements, strains, and stresses for triangular dislocation elements in a uniform elastic half space, *Comp. Geosci.,* **33,** 1064–1075.

Minoura, K., Imamura, F., Sugawara, D., Kono, Y. & Iwashita, T., 2001. The 869 Jōgan tsunami deposit and recurrence interval of large-scale tsunami on the Pacific coast of northeast Japan, *J. Nat. Dis. Sci.,* **23,** 83–88.

Miura, S., Iinuma, I., Yui, S., Uchida, N., Sato, T., Tachibana, K. & Hasegawa, A., 2006. Co- and post-seismic slip associated with the 2005 Miyagi-oki earthquake (M7.2) as inferred from GPS data, *Earth Planets Space,* **58,** 1567–1572.

Miura, S., Kodaira, S., Nakanishi, A. & Tsuru, T., 2003. Structural characteristics controlling the seismicity of southern Japan Trench fore- arc region, revealed by ocean bottom seismographic data, *Tectonophysics,* **363,** 79–102.

Miura, S., Takahashi, N., Nakanishi, A., Tsuru, T., Kodaira, S. & Kaneda, Y., 2005. Structural characteristics off Miyagi forearc region, the Japan Trench seismogenic zone, deduced from a wide-angle reflection and refraction study, *Tectonophysics,* **407,** 165–188.

Miyazaki, S., Segall, P., Fukuda, J. & Kato, T., 2004. Space time distribution of afterslip following the 2003 Tokachi-oki earthquake: implications for variations in fault zone frictional properties, *Geophys. Res. Lett.,* **31**(L06623), doi:10.1029/2003GL019410.

Nakanishi, A. *et al.*, 2004. Structural factors controlling the coseismic rupture zone of the 1973 Nemuro-Oki earthquake, the southern Kuril Trench seismogenic zone, *J. geophys. Res.,* **109**(B05305), doi:10.1029/2003JB002574.

Nakayama, W. & Takeo, M., 1997. Slip history of the 1994 Sanriku-Haruka-Oki, Japan, earthquake deduced from strong-motion data, *Bull. seism. Soc. Am.,* **87,** 918–931.

Namegaya, Y., Satake, K. & Yamaki, S., 2011. Fault models of the AD 869 Jogan earthquake: a possible predecessor of the 2011, off the Pacific Coast of Tohoku, earthquake, Abstract SE87-D5-PM2–102-018, in *Proceedings of the 8th Annual Meeting,* Asia Oceania Geoscience Society, Taipei, Taiwan.

Nanayama, F., Satake, K., Furukawa, R., Shimokawa, K., Atwater, B.F., Shigeno, K. & Yamaki, S., 2003. Unusually large earthquakes inferred from tsunami deposits along the Kuril trench, *Nature,* **424,** 660–663.

Nishimura, T., Nakahara, H., Sato, H. & Ohtake, M., 1996. Source process of the 1994 far east off Sanriku earthquake, Japan, as inferred from a broad-band seismogram, *Tohoku Geophys. J.,* **34,** 121–134.

Ortega Culaciati, F.H., Simons, M., Minson, S.E., Owen, S.E., Moore, A.W. & Hetland, E.A., 2011. A Bayesian analysis of the post-seismic deformation of the Great 11 March 2011 Tohoku-Oki (Mw 9.0) Earthquake: implications for future earthquake occurrence, in *EOS Trans., Abstract U53D-0094, AGU Fall Meeting*, San Francisco.

Owen, S.J., 2006. *CUBIT 10.2 Documentation,* pp. 532, Sandia National Laboratories, Albuquerque, NM, USA.

Ozawa, S., Nishimura, T., Suito, H., Kobayashi, T., Tobita, M. & Imakiire, T., 2011. Coseismic and postseismic slip of the 2011 magnitude-9 Tohoku-Oki earthquake, *Nature,* **475,** 373–376.

Peacock, S.M. & Wang, K., 1999. Seismic consequences of warm versus cool subduction metamorphism: examples from southwest and northeast Japan, *Science,* **286,** 937–939.

Perfettini, H. & Ampuero, J.-P., 2008. Dynamics of a velocity strenghtening region: implications for slow earthquakes and postseismic slip, *J. geophys. Res.,* **113**(B09411), doi:10.1029/2007JB005398.

Perfettini, H. *et al.*, 2010. Seismic and aseismic slip on the Central Peru megathrust, *Nature,* **465,** 78–81.

Pollitz, F.F., McCrory, P., Svarc, J. & Murray, J., 2008. Dislocation models of interseismic deformation in the western United States, *J. geophys. Res.,* **113**(B04413), doi:10.1029/2007JB005174.

Rani, S. & Singh, S.J., 1992. Static deformation of a uniform half-space due to a long dip-slip fault, *Geophys. J. Int.,* **109,** 469–476.

Rice, J., 1993. Spatio-temporal complexity of slip on a fault, *J. geophys. Res.,* **98,** 9885–9907.

Robinson, D.P. & Cheung, L.T., 2003. Source process of the Mw 8.3, 2003 Tokachi-Oki, Japan earthquake and its aftershocks, *Geophys. J. Int.,* **181,** 334–342.

Sagiya, T., 2004. A decade of GEONET: 1994–2003 – The continuous GPS observation in Japan and its impact on earthquake studies, *Earth Planets Space,* **56,** xxix–xli.

Satake, K., Hirata, K., Yamaki, S. & Tanioka, Y., 2006. Re-estimation of tsunami source of the 1952 Tokachi-oki earthquake, *Earth Planets and Space,* **58,** 535–542.

Savage, J.C., 1983. A dislocation model of strain accumulation and release at a subduction zone, *J. geophys. Res.,* **88,** 4984–4996.

Savage, J.C., 1995. Interseismic uplift at the Nankai subduction zone, Southwest Japan, 1951–1990, *J. geophys. Res.,* **100,** 6339–6350.

Savage, J.C., 1998. Displacement field for an edge dislocation in a layered half-space, *J. geophys. Res.,* **103,** 2439–2446.

Seno, T., Shimazaki, K., Somerville, P., Sudo, K. & Eguchi, T., 1980. Rupture process of the Miyagi-oki, Japan, earthquake of June 12, 1978, *Phys. Earth planet. Int.,* **23,** 39–61.

Shearer, P.M., 1999. *Introduction to Seismology,* 1st edn, Cambridge University Press, Cambridge, UK.

Shimazaki, K., 1974. Nemuro-Oki earthquake of June 17, 1973: a lithospheric rebound at the upper half of the interface, *Phys. Earth planet. Int.,* **9,** 314–327.

Simons, M. *et al.*, 2011. The 2011 magnitude 9.0 Tohoku-Oki Earthquake: mosaicking the megathrust from seconds to centuries, *Science,* **332,** 1421–1425, doi:10.1126/science.1206731.

Sladen, A. *et al.*, 2009. Source model of the 2007 Mw 8.0 Pisco, Peru earthquake—implications for seismogenic behavior of subduction megathrusts, *J. geophys. Res.,* **115,** doi:10.1029/2009JB006429.

Suwa, Y., Miura, S., Hasegawa, A., Sato, T. & Tachibana, K., 2006. Interplate coupling beneath NE Japan inferred from three-dimensional displacement field, *J. geophys. Res.,* **111**(B04402), doi:10.1029/2004JB003203.

Takahashi, N. *et al.*, 2004. Seismic structure and seismogenesis off Sanriku region, northeastern Japan, *Geophys. J. Int.,* **159,** 129–145.

Tanioka, Y., 2003a. Rupture area of the 1894 Nemuro-oki earthquake is larger than that of the 1973 Nemurooki earthquake, in *Japan Geoscience Union Meeting*, Japan, Abstract s208–007.

Tanioka, Y., 2003b. Source processes of the 1936 and 1978 Miyagi-oki earthquakes from the tsunami waveform analysis, in *Japan Geoscience Union Meeting*, Japan, Abstract s052–002.

Tanioka, Y., Ruff, L. & Satake, K., 1996. The Sanriku-Oki, Japan, Earthquake of December 28, 1994 (Mw 7.7): Rupture of a different asperity from a previous earthquake, *Geophys. Res. Lett.,* **23,** 1465–1468.

Townsend, J. & Zoback, M.D., 2006. Stress, strain, and mountain building in central Japan, *J. geophys. Res.,* **111**(B03411), doi:10.1029/2005JB003759.

Uchida, N., Nakajima, J., Hasegawa, A. & Matsuzawa, T., 2009. What controls interplate coupling?: evidence for abrupt change in coupling across a border between two overlying plates in the NE Japan subduction zone, *Earth planet. Sci. Lett.,* **283,** 111–121.

Umino, N. *et al.* 2006. Revisiting the three Mw7 Miyagioki earthquakes in the 1930s: possible seismogenic slip on asperities that were re-ruptured during the 1978 M = 7.4 Miyagi-oki earthquake, *Earth Planets Space,* **58,** 1587–1592.

UNAVCO, 2011. Plate Motion Calculator, Available at http://www.unavco.org/community_science/science-support/crustal_motion/dxdt/model.html10.1093/gji/ggs028.html (accessed 2 November 2012).

Yamanaka, Y. & Kikuchi, M., 2003. Source processes of the recurrent Tokachi-oki earthquake on September 26, 2003, inferred from teleseismic body waves, *Earth planet. Sci. Lett.,* **55,** e21–e24.

Yamanaka, Y. & Kikuchi, M., 2004. Asperity map along the subduction zone in northeastern Japan inferred from regional seismic data, *J. geophys. Res.,* **109**(B07307), doi:10.1029/2003JB002683.

Yoshii, T., 2005. Recent vertical Crustal Movement in theJapanese Islands as Deduced from GPS Observations (in Japanese), *Bull. Inst. Nat. Sci. Nihon Univ. Dept. Lit. Sci.,* **40,** 67–72.

APPENDIX A: ASPERITY CONFIGURATION AND PARAMETERS FOR THE JAPAN TRENCH MEGATHRUST

In this appendix, we discuss the methodology used to estimate the location and spatial extent of each inferred characteristic asperity on the Japan Trench megathrust surface, as well as its characteristic rupture interval. In determining these parameters, we try to honour, at a minimum, the latest significant ($M_w > 7.5$) ruptures inferred to have occurred on these asperities during the past century. We first present our analysis for the *M*7–8 class asperities from the southernmost asperity of our modelling domain (Fukushima) to the northernmost (Nemuro). We then discuss the two *M*9 asperities (Tohoku and Hokkaido) at the end of this appendix. A summary of estimated parameters is presented in Table 2, and the asperity configurations are presented in Fig. 1. In the calculations below, we use a convergence rate between the Pacific and Okhotsk plates of 8.3 cm yr^{-1} at the Japan Trench.We assume all asperities are ellipses on the megathrust, defined by the semi-major, r_{maj}, and minor, r_{min}, axes, and define the asperity aspect ratio, f, as r_{min}/r_{maj}. We assume $f = 0.8$ for all of the *M*7- and *M*8-class asperities for the purposes of mesh quality. We specify f for the *M*9 asperities below. The estimated size of the asperities depends on the plate velocity, V_P, moment, M_o, recurrence interval, ΔT_R, and f as

$$r_{maj} = \left(\frac{M_0}{\mu \pi f V_P (\Delta T_R)} \right)^{\frac{1}{2}}, \tag{A1}$$

where μ is shear modulus. The stress drop depends on M_o and asperity size according to

$$\Delta\sigma = \Theta(1). \left(\frac{M_0}{f (r_{maj})^3} \right), \tag{A2}$$

where $\Theta(1)$ is a factor whose value is typically of the order 1 [e.g. for a circular patch, $\Theta(1) = 7/16$ (Shearer 1999)]. We assume that the accumulated slip deficit is entirely relieved in each rupture, so that the characteristic slip is, $V_P \Delta T_R$.

Key uncertainties in the calculations are related to the choice of V_P and $\Delta\sigma$. We can get a feel for the sensitivity of asperity size to these two parameters, by taking the partial derivatives of r_{maj}:

$$\frac{\partial r_{maj}}{\partial V_P} = -\frac{1}{2V_P} \left(\frac{M_0}{\mu \pi f V_P \Delta T_R} \right)^{\frac{1}{2}} = -\frac{r_{maj}}{2V_P} \Rightarrow \frac{\Delta r_{maj}}{r_{maj}} = -\frac{\Delta V_P}{2V_P} \tag{A3}$$

and,

$$\frac{\partial r_{maj}}{\partial(\Delta\sigma)} = -\frac{1}{3(\Delta\sigma)} \left(\frac{M_0}{f \Delta\sigma} \right)^{\frac{1}{3}} = -\frac{r_{maj}}{3(\Delta\sigma)}$$

$$\Rightarrow \frac{\Delta r_{maj}}{r_{maj}} = -\frac{\Delta(\Delta\sigma)}{3(\Delta\sigma)}, \tag{A4}$$

and thus, for a 10 per cent variation in V_P (e.g. 8–9 cm yr^{-1} depending on the reference frame used here), our estimate of r_{maj} varies by about 5 per cent and stress-drop by about 15 per cent. Also, for a fixed ΔT_R, a 10 per cent variation in V_P results in a 10 per cent variation in the estimated characteristic slip for each rupture.

A.1 Fukushima-oki—ruptures of 1938

On the megathrust interface off Fukushima, three large events occurred in close succession: M_w7.4 (1938 May), M_w 7.7 and M_w 7.8 (both in 1938 November). On the scale of simulating an entire seismic cycle (∼100 yr), the moment release from these three events can be considered instantaneous. Using the estimated moments of the each of the events from long-period surface waves (Abe 1977), the combined moment release from these three events is M_0, of 1.6×10^{21} N m, equivalent to a moment-magnitude, M_w, of 8.1. Since there has not been a $M_w > 7$ earthquake off Fukushima since 1938, we assume a recurrence interval of ∼75 yr similar to the value assumed for the Tokachi-Oki region (Yamanaka & Kikuchi 2003). Using this ΔT_R in eqs (A1) and (A2), assuming that the combined moment in the 1938 events is characteristic, we find $r_{maj} \approx 60$ km and $\Delta\sigma \approx 10$ MPa. The latter is at the upper-bound of observed seismic stress-drops (Kanamori & Anderson 1975). In comparison, Abe (1977) estimated stress-drop, $\Delta\sigma$, to be in the range ∼ 2.8–5.6 MPa from locally high-slip patches. If on the other hand, we assume an equivalent single characteristic elliptical asperity with $\Delta\sigma \sim$ 1 MPa, then $r_{maj} \approx 126$ km, resulting in a characteristic asperity area of about 4×10^4 km^2. This area is almost three times larger than that estimated for the combined total area for all three events by Abe (1977). Moreover, because we are assuming the same characteristic slip for every rupture on each asperity, the corresponding rupture interval is then about 16 yr. A characteristic repeat time this low is inconsistent with the known earthquake record, and thus we assume the larger stress-drop above.

A.2 Miyagi-oki—ruptures of 1936, 1978 and 2005

Umino *et al.* (2006) infer that three ruptures on this asperity occurred in the mid-1930s: in 1933, 1936 and 1937, with a combined moment release of 2.6×10^{20} N m (equivalent to M_w 7.5). These ruptures overlapped with the western, central and eastern portions of the M_w7.5 1978 rupture area, but with a moment that was only one-third of that for the latter event (Tanioka 2003b). The 2005 rupture also partially overlapped with the updip (southeastern) portion of the 1978 rupture area (Miura *et al.* 2006). We assume the 1978 M_w 7.4–7.5 event as the characteristic earthquake for this region with $M_0 = 1.7$–3×10^{20} N m. The latter is based on moment estimates from tsunami data (Tanioka 2003b) and long-period surface waves (Seno *et al.* 1980). The 2005 event was estimated to be M_w 7.2 event ($M_0 = 1.7$–7×10^{19}) from GPS and seismic data (Miura *et al.* 2006). We assume a single Miyagi asperity in our simulations, and based on the 1933–1937 sequence and the 1978 event, we assume $\Delta T_R = 40$ yr for characteristic ruptures on this asperity. This rupture recurrence results in $r_{maj} \approx 35$ km and $\Delta\sigma \approx 9$ MPa, which is near the upper-bound of observed seismic stress-drops (Kanamori & Anderson 1975). In comparison, the stress drops for the 1978 and 2005 events were estimated to be in the 10–15 MPa range based on localized high-slip patches (Seno *et al.* 1980; Tanioka 2003b). The 2005 event may be consistent with the 1933–1937 sequence in that it ruptured only one part of the characteristic asperity, and subsequent events may follow to rupture the rest of the characteristic asperity.

Another way to estimate the characteristic size for Miyagi asperity is to assume that the mean stress-drops and asperity shapes in the 2005 and 1978 events are similar. An estimate can then be made of the 1978 characteristic asperity size relative to the well-determined asperity size for the 2005 M_w7.2 event $r_{maj} \approx 22$ km by

$$\Delta\sigma_{1978} = \Delta\sigma_{2005} = \Theta(1). \left(\frac{M_0^{(1978)}}{f (r_{maj,1978})^3} \right) = \Theta(1).$$

$$\left(\frac{M_0^{(2005)}}{f (r_{maj,2005})^3} \right) \Rightarrow r_{maj,1978} = r_{maj,2005} \left(\frac{M_0^{(1978)}}{M_0^{(2005)}} \right)^{\frac{1}{3}} \approx 35 \text{ km},$$

which is identical to that estimated from the assumed recurrence interval of 75 yr. Had we assumed a characteristic elliptical asperity having a much lower mean stress drop, $\Delta\sigma \sim 1$ MPa, then the semi-major asperity dimension would almost double (∼70 km), with a rupture interval that is only one-fourth (∼10 yr) of the value inferred above from observations.

A.3 Sanriku-oki—ruptures of 1931, 1968 and 1994

The location and size of the 1994 M_w 7.8 event off Sanriku were determined using strong-motion (Nakayama & Takeo 1997), and broad-band (Nishimura *et al.* 1996) data, while for the 1968 M_w 8.2 event, rupture location and size were estimated using *P* wave first motions as well as long-period surface waves (Kanamori 1971). Based on focal mechanisms, the deeper part of the 1968 event may not even be on the subduction megathrust (Hiroo Kanamori, personal communication, 2009), and we consider only the 1994 rupture area as the characteristic asperity. Using $M_0 = 3\text{–}4\times10^{20}$ N m as the moment of the 1994 event (Nishimura *et al.* 1996; Tanioka *et al.* 1996; Nakayama & Takeo 1997) and $\Delta T_R = 30$ yr (approximate mean value of rupture intervals between 1931, 1968 and 1994 events), we find $r_{maj} \approx 45$ km and $\Delta\sigma \approx 5$ MPa. This stress drop is in the middle of the range of observed seismic stress-drops (Kanamori & Anderson 1975). Again, had we assumed a characteristic elliptical asperity with a lower mean stress drop, $\Delta\sigma \sim 1$ MPa, the estimated recurrence interval (∼12 yr) would be too small to explain the recent rupture history in this region.

A.4 Tokachi-oki—ruptures of 1952 and 2003

Studies comparing sizes of the 1952 and 2003 ruptures off Tokachi determined that the latter event was either slightly smaller, or roughly equal in size to the former event, with nearly coincident rupture areas. The 2003 event was estimated to be M_w8.0 from tsunami waveform modelling (Satake *et al.* 2006), and re-estimation of 1952 aftershock pattern (Hamada & Suzuki 2004), but M_w8.2 (similar to that for the 1952 event), from broad-band SH & long-period mantle phases (Robinson & Cheung 2003), as well as joint inversion using strong-motion and GPS (Koketsu *et al.* 2004). Using the better-constrained and more recent estimates of the magnitude of the 2003 event, $M_0 \sim 2\times10^{21}$ N m for Tokachi-Oki (e.g. Koketsu *et al.* 2004).Robinson & Cheung (2003) estimated that the mean stress drop in the 2003 event was 0.5 MPa, but that stress drop was 10–25 MPa on localized high-slip regions in the rupture. They also estimated the mean slip to be about 2.2 m. Assuming that the 1952 and 2003 events ruptured the same characteristic asperity with $\Delta T_R = 50$ yr, $r_{maj} \approx 80$ km and $\Delta\sigma \approx 5$ MPa. This stress drop is within the observed range of seismic stress-drops (Kanamori & Anderson 1975), and reasonable given estimates of stress drop in the 2003 event (Robinson & Cheung 2003). If we assume that the rupture area of the 1952 and 2003 events were not equal, but that the ruptures were both elliptical with the same aspect ratio and that the mean stress-drops were the same, then the characteristic semi-major asperity dimension relative to the well determined rupture dimension of the 2003 event ($r_{maj} \approx 70$ km) would be

$$\Delta\sigma_{1952} = \Delta\sigma_{2003} = \Theta(1).\left(\frac{M_0^{(1952)}}{f(r_{\mathrm{maj},1952})^3}\right) = \Theta(1).$$
$$\left(\frac{M_0^{(2003)}}{f(r_{\mathrm{maj},2003})^3}\right) \Rightarrow r_{\mathrm{maj},1952} = r_{\mathrm{maj},2003}\left(\frac{M_0^{(1952)}}{M_0^{(2003)}}\right)^{\frac{1}{3}} \approx 75 \text{ km}. \quad \text{(A6)}$$

This second estimate of asperity size it similar to that estimated using the assumed recurrence interval above. Our estimate of the along-strike length of the asperity of about 150 km ($2 \times r_{maj}$) also agrees well with the width between two subduction zone geologic features that seem to bound this rupture area: Kushiro canyon to the east, and the plate bend with deepening of continental shelf to the west (Hamada & Suzuki 2004). Assuming a lower mean stress drop of 1 MPa results in an asperity almost twice as large and a recurrence interval of only a third of the observed.

A.5 Nemuro-oki—rupture of 1973

Great earthquakes occurred off Nemuro in 1894 and 1973, but the latter event is estimated to have been much smaller than the 1894 event (Tanioka 2003a). It is conjectured that the 1894 event ruptured the source areas of both the 1973 Nemuro-oki and 1952 Tokachi-oki events (Tanioka 2003a). The 1973 event has been estimated to be between M_w 7.8 [$M_0 \sim 5\times10^{20}$ N m (Tanioka 2003a)], and M_w 7.9 [$M_0 \sim 6.7 \times 10^{20}$ N m (Shimazaki 1974)]. We adopt the more recent moment estimate from Tanioka (2003a), along with their estimate of mean fault slip of ∼ 2 m. In contrast, Shimazaki (1974) estimated a slip of 1.6 m, and mean stress drop of 3.5 MPa. Here, we assume a rupture interval of about 40 yr (similar to the Miyagi-oki region adjacent to the Fukushima asperity). Such a rupture interval results in $r_{maj} \approx 45$ km and $\Delta\sigma \approx 7$ MPa. If we assume the 1894 event completely ruptures the 1973 asperity, taking $\Delta T_R =$ 75 yr as in the Tokachi-Oki area (Yamanaka & Kikuchi 2003), we find $\Delta\sigma$ is almost two and half times larger, beyond the upper bound for observed seismic stress-drops (Kanamori & Anderson 1975). As with previous asperities, assuming a much smaller mean characteristic stress drop of 1 MPa results in a recurrence interval of only ∼11 yr.

A.6 Tohoku_*M*9: M_w 9 class asperity equivalent to the Tohoku-oki rupture of 2011 March

Estimates of moment magnitude for the 2011 March mega-earthquake off the Sendai coast range from 8.8 to 9.2 ($M_0 \sim 2$ to 7×10^{22} N m) and estimated static stress drops lie between 2 and 10 MPa (Simons *et al.* 2011). For the simulations in this paper, we choose a value of $M_0 \sim 4.5\times10^{22}$ N m *(*M_w 9.1) as the characteristic rupture size for this region. Minoura *et al.* (2001) have documented two separate tsunamis along the Sendai coastline and attribute it to two *M*8 class earthquakes in AD 869 (Jogan earthquake) and AD 1611. However, there are large uncertainties in these magnitudes, and these two events could have been much bigger. In addition, the location of theses two tsunamigenic events is not well constrained. Since our simulations assume periodic ruptures of each asperity, if we consider that the 1611 event ruptured the Tohoku *M*9 asperity, we would infer a rupture interval of 400 yr between the 1611 and 2011 ruptures. Using a 400-yr rupture recurrence, our simulations would include another *M*9 rupture in the 1200s, as well as simulate the 869 Jogan event decades earlier than it actually occurred. If on the other hand, we consider that the 1611 tsunami resulted from a rupture of another, *M*8- or *M*9-class, asperity (e.g. the Hokkaido asperity described in the next section), we would assume $\Delta T_R =$ 1140 yr, based solely on the Jogan and 2011 events. We tested simulations with rupture intervals of the Tohoku asperity of 500 and 750 yr, but found that our major conclusions regarding interseismic slip-deficits and predicted vertical subsidence along the east coast of northern Japan over the past century remain unchanged.We

assume an elliptical asperity, with $f = 0.35$, roughly based on the observed coseismic slip distribution for this earthquake based on the most recent 2011 event. This aspect ratio also avoids physical overlap with the Miyagi and Fukushima asperities. We then find $r_{\rm maj} \approx 120$ km and $\Delta\sigma \approx 60$ MPa, which is consistent with the observed high mean stress for the 2011 Tohoku $M_{\rm w}$ 9 event (Simons *et al.* 2011). Assuming a more typical stress-drop of 10 MPa (Kanamori & Anderson 1975), we would infer an asperity semi-major dimension of 150 km and a rupture interval of ∼300 yr. No earthquakes with $M_{\rm w} \geq 8$, or resulting tsunamis, have been documented for the Sendai region in the past 300 yr, and we argue that a recurrence interval of 300 yr is too short. In addition, results from tsunami inundation modelling of the Jogan earthquake estimate a potential source area located approximately over the same region of the megathrust, albeit smaller, as slipped in the 2011 $M_{\rm w}$ 9 Tohoku-oki rupture (Namegaya *et al.* 2011). Therefore, we take the past rupture history to be the strongest constraint in determining the size and recurrence interval of the Tohoku *M*9 asperity. Further, in order make sure that the modelled *M*8-class Fukushima asperity ruptures each time this much larger *M*9-class asperity ruptures, as well as achieve practical simulation times for a single CRS (Section 2.2), we chose a rupture interval for the Tohoku-oki event of 1125 yr. For the purpose of keeping computational costs reasonable, we do not try to synchronize ruptures of the much smaller *M*7-class Miyagi-oki asperity with those of the Tohoku-oki asperity. However, in our model simulations, such coincident ruptures of the *M*7 & *M*9-class asperities off Tohoku occur every 9000 simulated years (i.e. after a set of every 8 *M*9-class ruptures, or every 225 *M*7-class ruptures).

A.7 Hokkaido_*M*9: Tsunamigenic $M_{\rm w}$ 9 class asperity off Hokkaido

Nanayama *et al.* (2003) document evidence of large tsunamis due to large earthquakes roughly every 500 yr off of Hokkaido and Kuriles over the past several thousand years. They speculate that these mega-earthquakes involve rupture of spatially extensive shallow tsunamigenic asperities, in addition to slip in deeper asperities that also rupture more frequently in $M_{\rm w}$ 8 earthquakes (e.g. Tokachi and Nemuro asperities). They estimate that the last such mega-earthquake occurred before 1660. Here, we assume that the potency of such a large shallow tsunamigenic asperity off of Hokkaido is similar to that for the Tohoku *M*9 asperity (Section A.6), but rupturing with a characteristic recurrence interval of 500 yr. We take $f = 0.25$ to avoid overlap with nearby asperities, $M_{\rm o} = 3.46\times10^{22}$ N m, and $\Delta T_{\rm R} = 500$ yr to find $r_{\rm maj} \approx 175$ km and $\Delta\sigma \approx 26$ MPa. Choosing a 500-yr recurrence for ruptures of the Hokkaido asperity ensures that the modelled Tokachi *M*8-class asperity also ruptures with this larger asperity. However, similar to the problem of synchronizing the Miyagi-oki with Tohoku *M*9 asperity, it is hard to synchronize ruptures of the Hokkaido asperity with ruptures on the much smaller *M*7-class Nemuro asperity. The closest in time that the Hokkaido and Nemuro asperities rupture is ±5 yr (given the assumed times, $T_{\rm R}$ of their latest ruptures, and assuming 5 yr round-off).

APPENDIX B: NUMERICAL SOLUTION PROCEDURE, COMPUTATIONAL EXPENSE AND CONVERGENCE

To estimate slip evolution on the fault surface, we solve the discretized traction evolution equation that accounts for ongoing forward slip along the fault interface, continuous far-field plate loading (represented as a backslip rate along the interface), and the cumulative coseismic slip on all asperities (e.g. Rice 1993; Hetland *et al.* 2010)

$$\tau_i = (s_j - tV_j)K_{ji} + \sum_a S_a K_{ai}, \tag{B1}$$

where $K_{\rm ji}$ are the traction kernels (i.e. tractions at patch *i* due to slip on patch *j*), $V_{\rm j}$ is the backslip rate on the *j*th patch (equivalent to the effect of far-field plate loading), $S_{\rm a}$ is the characteristic coseismic slip on all patches comprising asperity *a*, and traction (τ), and slip (s) vary both in space and in time. Table 1 summarizes the notation used in this study. For a point located within an asperity, accumulated stresses are released only coseismically, while for a point located outside an asperity, stresses are relaxed throughout the interseismic period. Surface displacements are given by

$$u_k = (s_j - tV_j)G_{jk} + \sum_a S_a G_{ak}, \tag{B2}$$

where $G_{\rm jk}$ are the surface displacement kernels (or Green's functions, i.e. displacements at observation station *k* due to slip on patch *j*). We use triangular dislocation solutions for the elastic half-space (Comninou & Dunders 1975; Meade 2007) to compute both traction and displacement kernels.We only consider rate-strengthening rheologies. Specifically, we consider a regularized functional representation (e.g. Rice 1993)

$$\dot{s} = V_0 e^{\left(\frac{-f_0}{(a-b)}\right)} \sinh\left(\frac{\tau}{(a-b)\sigma_0}\right), \tag{B3}$$

where, f_0 is the static coefficient of friction, a and b are the coefficients of the direct and indirect (state-dependent) dynamic frictional effects and σ_0 is the effective normal traction on the fault surface. All simulations are carried out using a non-dimensional parametrization (see Hetland *et al.* (2010) for details). For the rate-strengthening relationship above, there are two composite rheological parameters: $\rho = f_0/(a-b)$, and $\alpha = (a-b)\sigma_0$. The first parameter is already dimensionless, and the second can be non-dimensionalized using,

$$\alpha_0 = \tau_0 = \frac{\mu S_0}{D_0}, \tag{B4}$$

where S_0 is the characteristic slip on the asperity and D_0 is the characteristic asperity dimension (assumed to be that of the largest asperity in the simulation). The resulting non-dimensional form of eq. (B3) becomes,

$$V' = \frac{\dot{s}}{V_0} = f(\tau', \alpha') = e^{-\rho} \sinh\left(\frac{\tau'}{\alpha'}\right), \tag{B5}$$

where, V_0 is the plate loading rate (plate velocity), and $\alpha' = \alpha/\alpha_0$. We impose a narrow slip transition zone around each asperity, over which coseismic slip tapers off to zero. The effect of different parametrizations for the slip distribution in this transition zone (or 'slip-tapering') are discussed in Hetland *et al.* (2010). Here, we choose a half-Gaussian coseismic slip-taper around the asperities. The quasi-static equilibrium equation (eq. B1) and the constitutive relation (eq. B3) are integrated over time using an adaptive time-step Runge-Kutta integration scheme (Hetland *et al.* 2010).

In our models, we allow the much larger *M*8-class asperities to rupture every time the *M*9-class asperities rupture (i.e. *M*9 rupture intervals are integral multiples of those for adjacent *M*8s). Such an assumption for *M*8- or *M*9-class asperities is justified considering the large uncertainty in historic ruptures for these asperities. We note that as a consequence of our assumption of fixed asperity rupture intervals, and that the Sanriku-oki asperity last ruptured in 1994,

the penultimate earthquake in 1968 on this asperity is modelled 4 yr earlier than it actually occurred (based on its rupture interval in Table 2; see Fig. 3-inset). However, the 1968 event is far enough removed from the GPS velocity window that uncertainties of a few years in rupture time do not seem to affect velocity predictions significantly. This weak influence of ruptures prior to the most recent one is another reason for not considering non-characteristic slip, especially on the small *M*7-class asperities.

Our current forward models are computationally expensive. The spin-up of each of the APRE simulations from zero initial stresses (Section 2, Fig. 3) takes about a week on a 2011 MacPro workstation. The long spin-up time is due to the complex rupture sequences involving multiple asperities, as well as the high slip-rates over the free surface extension (FSE) immediately following ruptures on any of the asperities. The APOST simulations take much longer, because of the large number of ruptures on the *M*7- and *M*8-class asperities between each *M*9-class rupture. Therefore, to keep computational costs manageable for the APOST simulations, we prestress the megathrust with the mean equilibrium tractions required for steady subduction, τ_{eq} (Section 2.3). However, even prestressed models need to spin-up as the fault tractions adjust to the imposed ruptures. In addition, even after spin-up, any model needs to be run until the CRS, comprising the most recent ruptures on all model asperities, has been simulated (Fig. S1, and Fig. 3-inset).

An important issue for determining the accuracy of model predictions is whether the driving coseismic stresses, as well as postseismic slip, are accurately resolved by a given discretization (or mesh). The goal of convergence tests is to better resolve these coseismic tractions driving fault slip, and thus more accurately compute the predicted surface velocities after model spin-up. Formal convergence tests for the complex multi-asperity rupture sequence scenarios presented in the main paper can be very time-consuming, especially for frictional rheologies. So we carried out convergence tests for a less complex problem: a triangular discretization of the 3-D megathrust interface having a linear viscous rheology, and only two of the asperities—Miyagi and Sanriku—which are common to both APRE and APOST scenarios. We generated higher resolution geometry-adaptive meshes that had essentially the same number of coarse elements near the periphery of the model domain, but significantly more elements in the vicinity of asperities (locations of peak driving tractions). Using these higher resolution meshes, the spun-up model predictions did indeed converge with increasing mesh resolution. Furthermore, model predictions using the 'coarsest' meshes (such as those presented here) were not significantly different from those using the 'finest' meshes—indicating that the mesh used in this study (Fig. 1) does sufficiently resolve the driving stresses and fault slip evolution. We confirmed the insensitivity of our fault slip distribution over the interseismic period to minor geometric perturbations by testing several variants of both asperity configurations having slightly different asperity locations and extents.

SUPPORTING INFORMATION

Additional Supporting Information may be found in the online version of this article:

Figure S1. (a) Synthetic rupture sequence for the APOST configuration. Time (*x*-axis) is normalized by the fixed rupture interval of the largest asperity ('Tohoku-M9', maroon circles), $\Delta T_{R,Tohoku9} =$ 1125 yr. This complex rupture sequence is generated by assuming that all model asperities rupture at fixed intervals given in Table 2. All asperities are numbered as in Table 2 and Fig. 1. Each filled circle represents a rupture, with its size and colour indicating characteristic rupture magnitude. The current rupture sequence (CRS, red rectangle), containing the latest ruptures on all of the APOST asperities (observed or inferred), repeats every $8\Delta T_{R,\,Tohoku9}$, or 9000 yr (and corresponds to the last ΔT_R of this time-interval). Yellow shaded patch indicates the time-period shown in (b). (b) Zoom-in of the CRS over a 60-yr time interval prior to the GPS observation period (1996–2000, green shading). Only asperities that ruptured during this time interval are shown.

Figure S2. Observed GPS velocities (left column: top and middle panels) and corresponding dilatation-rates (left column: bottom panel) compared with model predictions (middle column) and residuals (observed—modelled, right column) for the APRE configuration and assuming a frictionless fault, *APRE*-α0. Magnitude of mean residual velocity, $|\delta V|$, is shown at the top of the right column. Plate convergence velocity vector is shown in each panel for scale. The scale for principal strain crosses is shown in each of the bottom panels. Green stars represent the epicentres of major recorded earthquakes during the past 75 yr. Yellow star in the left column represents the reference station (Geonet #940034).

Figure S3. Observed GPS velocities (left column: top and middle panels) and corresponding dilatation-rates (left column: bottom panel) compared with model predictions (middle column) and residuals (observed–modelled, right column) for the APRE configuration and weak rate-strengthening rheology, *APRE*-α0.01. All scales and symbols are identical to that for Fig. S2.

Figure S4. Observed GPS velocities (left column: top and middle panels) and corresponding dilatation-rates (left column: bottom panel) compared with model predictions (middle column) and residuals (observed–modelled, right column) for the APRE configuration and strong rate-strengthening rheology, *APRE*-α0.10. All scales and symbols are identical to that for Fig. S2.

Figure S5. Observed GPS velocities (left column: top and middle panels) and corresponding dilatation-rates (left column: bottom panel) compared with model predictions (middle column) and residuals (observed–modelled, right column) for APOST configuration and assuming a frictionless fault, *APOST*-α0. All scales and symbols are identical to that for Fig. S2.

Figure S6. Observed GPS velocities (left column: top and middle panels) and corresponding dilatation-rates (left column: bottom panel) compared with model predictions (middle column) and residuals (observed–modelled, right column) for the APOST configuration and weak rate-strengthening rheology, *APOST*-α0.01. All scales and symbols are identical to that for Fig. S2.

Figure S7. Observed GPS velocities (left column: top and middle panels) and corresponding dilatation-rates (left column: bottom panel) compared with model predictions (middle column) and residuals (observed–modelled, right column) for the APOST configuration and strong rate-strengthening rheology, *APOST*-α0.10. All scales and symbols are identical to that for Fig. S2 (http://gji.oxfordjournals.org/lookup/suppl/doi:10.1093/gji/ggs028/-/DC1).

Please note: Oxford University Press are not responsible for the content or functionality of any supporting materials supplied by the authors. Any queries (other than missing material) should be directed to the corresponding author for the article.